energies

MDPI

Article

Generic EMT Model for Real-Time Simulation of Large Disturbances in 2 GW Offshore HVAC-HVDC Renewable Energy Hubs

Saran Ganesh [1], Arcadio Perilla [1], Jose Rueda Torres [1,*], Peter Palensky [1], Aleksandra Lekić [1] and Mart van der Meijden [1,2]

[1] Department of Electrical Sustainable Energy, Delft University of Technology, Mekelweg 4, 2628 CD Delft, The Netherlands; S.GANESH-2@student.tudelft.nl (S.G.); A.Perilla@tudelft.nl (A.P.); P.Palensky@tudelft.nl (P.P.); A.Lekic@tudelft.nl (A.L.); Mart.vander.Meijden@tennet.eu (M.v.d.M.)
[2] TenneT TSO B.V., 6812 AR Arnhem, The Netherlands
* Correspondence: J.L.RuedaTorres@tudelft.nl

Abstract: This paper proposes a Electro-Magnetic Transient (EMT) model of a 2 GW offshore network with the parallel operation of two Modular Multi-level Converter (MMC)—High Voltage Direct Current (HVDC) transmission links connecting four Offshore Wind Farms (OWFs) to two onshore systems, which represent a large scale power system. Additionally, to mitigate the challenges corresponding to voltage and frequency stability issues in large scale offshore networks, a Direct Voltage Control (DVC) strategy is implemented for the Type-4 Wind Generators (WGs), which represent the OWFs in this work. The electrical power system is developed in the power system simulation software RSCAD^{TM}, that is suitable for performing EMT based simulations. The EMT model of 2 GW offshore network with DVC in Type-4 WGs is successfully designed and it is well-coordinated between the control structures in MMCs and WGs.

Keywords: large scale offshore network; direct voltage control; EMT; MMC; HVDC

Citation: Ganesh, S.; Perilla, A.; Rueda Torres, J.; Palensky, P.; Lekić, A.; van der Meijden, M. Generic EMT Model for Real-Time Simulation of Large Disturbances in 2 GW Offshore HVAC-HVDC Renewable Energy Hubs. *Energies* **2021**, *14*, 757. https://doi.org/10.3390/en14030757

Academic Editor: Georgios Konstantinou
Received: 30 November 2020
Accepted: 22 January 2021
Published: 1 February 2021

1. Introduction

According to the Paris Agreement, the European Union's (EU) should contribute in reduction of greenhouse gas emissions by at least 40% by 2030 when compared to 1990 [1]. The plans involve a future target between 70 GW to 150 GW offshore wind power installed in the North Sea by 2040. The latest European Commission prediction estimates installation of 140 to 450 GW offshore wind power in the EU by 2050. With the current pace, the rate of offshore wind energy deployment is deficient in comparison to the Paris Agreement objectives [1]. To comply with these objectives, an extraordinary jump in offshore wind energy is required. A practical solution calls for an increase in large scale offshore wind energy deployment in the North Sea [2]. As the part of the North Sea Wind Power Hub Programme [3], the Transmission System Operator (TSO) of the Netherlands, TenneT, has already entered into an innovation partnership with its suppliers to establish a 2 GW offshore platform. Likewise, Denmark is progressing with the first hub-and-spoke energy island with a vision of connecting at least 10 GW of offshore wind power in the North Sea [4].

Currently, the state-of-the-art technology for the transfer of offshore wind power to the onshore system are Voltage Source Converter (VSC) based-HVDC transmission links. Presently, MMC topology, that falls under the classification of VSC topologies, is the most suitable solution. Advantages of the MMC are [5]: (1) ease of integration with OWFs, (2) support of the bi-directional power flow between the offshore network and onshore system, and (3) independent control of active and reactive powers in the network. However, with the available technology, MMC-HVDC transmission are limited to a rated capacity of 1.2 GW [6].

The implementation of large scale offshore networks (greater than or equal to 2 GW) creates a highly Power Electronic (PE) converter dominated network. The absence of conventional generators would mean that the PE converters will have to take into account the decreasing inertia of the system that leads to faster dynamic behaviour, and it requires controllers with shorter time response. The challenges in design of PE converters' voltage and frequency controls, without conventional units, are prominent in large scale offshore networks. Moreover, distant OWFs would be connected in parallel. With the parallel operation of the conventional current controllers in WGs, interactions can persist among them and could lead to instability of the network. Additionally, the restoration of the grid, following disturbances by the PE converter units, is a serious matter of concern. With the conventional current control approach, grid restoration is challenging without the help of auxiliary diesel generators. However, in the case of large scale offshore networks, PE converters take the role of grid restoration. There can be arguments that storage facilities such as battery and thermal can be a realizable solution in case when there are no conventional generators available. Huge investment costs, low lifetime and low efficiency when compared to controller modifications are the drawbacks that make these storage facilities practically unusable in large scale offshore networks [7].

Conventionally, the OWFs are coupled to an AC collector platform through 33 kV High Voltage Alternating Current (HVAC) cables. The voltage is stepped-up to 145 kV using a power transformer at the collector platform, and power is transferred to the offshore converter station using 145 kV HVAC cables. However, in the upcoming projects, the rated voltage levels are expected to increase from 33 kV to 66 kV to avoid the use of a collector platform and to directly transfer power from OWFs to the offshore converter station using 66 kV HVAC cables. Hence, it is necessary understand the performance of large scale offshore networks developed with 66 kV voltage rating.

With the available MMC-HVDC transmission technology, multiple MMC-HVDC transmission links connected in parallel would be required to transfer the bulk amount of offshore wind power generated from large scale offshore networks to the onshore system. The power flow between the parallel operated MMCs and the OWFs must be coordinated both during steady state and dynamic conditions. The major challenges regarding voltage and frequency control during islanding of the OWFs must be taken into account. The scenario of reactive current injection that needs to be provided by the WGs during dynamic conditions must also be taken into consideration [8]. Therefore, the progress towards the development of large scale offshore networks calls for a generic model with a suitable layout and available technology that is capable of tackling the aforementioned technical challenges and providing stable operation during steady state and dynamic conditions.

This paper adopts the latest trend in technology, and achieves the overall goal of developing a generic EMT model of 2 GW, 66 kV HVAC offshore network in RSCAD. The performance of the model is analyzed based on the voltage and active power values at various locations in the network for highly severe dynamic conditions. The EMT model developed in this paper adopts a modified layout with two MMCs working in parallel and connecting four OWFs to the onshore system. The layout of the 2 GW offshore network is achieved using hub-and-spoke principle from [9] which involves connecting an offshore "hub" to several onshore grids in same or different areas through "spokes". Additionally, the technical challenges faced while using conventional current control strategies in WGs, related to voltage and frequency control, are mitigated by implementing DVC from [10] in all Type-4 WGs in RSCAD for real-time application. The novelty of the paper lies in the implementation of DVC in four WGs in parallel operation and work in coordination with two MMCs with different control strategies during steady-state and dynamic conditions in the network.

The sections of the paper are arranged as follows. In Section 2, the processors available for modelling in RSCAD are described. Furthermore, it is given the topology selected for the 2 GW offshore network. Section 3 describes the model layout of the 2 GW offshore network. The control structures utilized in the 2 GW offshore network are discussed in

Section 4. Section 5 depicts preset conditions before the start of the simulation of the model, the synchronization of the offshore converter stations, and the energization of the HVAC cables and OWFs. It also employs the dynamic performance analysis for the 2 GW EMT model. Section 6 concludes the paper.

2. Defining the Layout for the 2 GW Offshore Network

The initial aspect of an offshore network is the topology of the network. The MMC, due to its improved controllability and superior system performances, has been often employed for MMC-HVDC transmission for integration of the distant OWFs. For the connection of new OWFs in the vicinity of the already existing ones, parallel operation of MMC-HVDC transmission systems can be constructed. It is expected that in the near future will be used parallel MMC-HVDC to create multiple connections to the onshore system. Thus, the interest in hybrid systems with the hub-and-spoke principle proposed by ABB [9] has been increased. It is represented in Figure 1. In the Figure 1a is depicted connection of OWFs to an offshore converter station, which in turn transfers power to the onshore system through multi-terminal HVDC connections. However, the scaling of offshore wind power is limited to the installed capacity of MMC unit in such a layout. Another layout involves the OWFs connected through AC links to a back-to-back HVDC converter station as shown in Figure 1b. Long distance HVAC transmission is required for the transfer of power from OWFs to the onshore network, and hence, it contributes to high losses in the network when compared to HVDC transmission for larger distances. Figure 1c represents the connection of multiple OWFs to the offshore converter station, where the power is transferred to the onshore system through multiple HVDC links. This layout provides contingency in the network by supplying offshore wind power to at least one onshore system if one of the HVDC links gets disconnected [11]. A stage-wise construction of such a HVDC project is easier to be achieved by the developers as well [5].

A specific configuration for a 2 GW offshore network is currently non-existent, and this paper tries to fill this research gap. This paper expands the single OWF model from [12] to create 2 GW offshore wind power network. This is possible by connecting four OWF models, each generating power of ∼500 MW, in parallel. The reason for choosing four OWFs is to ensure a symmetrical layout and to test the ability of RSCAD to perform simulations on such configuration. Correspondingly, a 2 GW offshore converter station capacity is required to transfer the generated amount of power to the onshore system. However, currently deployed (state-of-the-art) MMC-HVDC transmission, has a maximum rated capacity of 1.2 GW [6]. Hence, with the available technology, two MMC offshore stations of 1 GW each will be required for 2 GW power transmission. Taking the aforementioned factors into account, a modified layout of Figure 1c is developed for this work.

2.1. Scaling of Single OWF Model for 2 GW Offshore Network

The 2 GW offshore network is modelled using RSCAD simulation tool which runs on Real Time Digital Simulator (RTDS) clusters. RSCAD simulations can be run either using NovaCor or PB5 processor cards. For this workd is chosen NovaCor processor, because it has 2–3 times higher simulation capacity than completely loaded PB5 processor [13]. For an extensive power system network, NovaCor processor requires distribution of the system into subsystems. RSCAD allows provision for splitting of the network into subsystems if the network is large. This feature is utilized using Tline modules, that are used to connect subsystems, which is explained in Section 3.2 in detail.

There are two NovaCor processors available at TU Delft, and they are equipped with four cores each. These cores are utilized to solve the overall network solution, auxiliary components (such as transformers, cables, generators etc.) and the controls present in the simulation. Assignment of cores for solving various components of the network is an important step that needs to be considered while modelling, as they depict the total load that is distributed over the available cores. The process is detailed in Section 3.1.

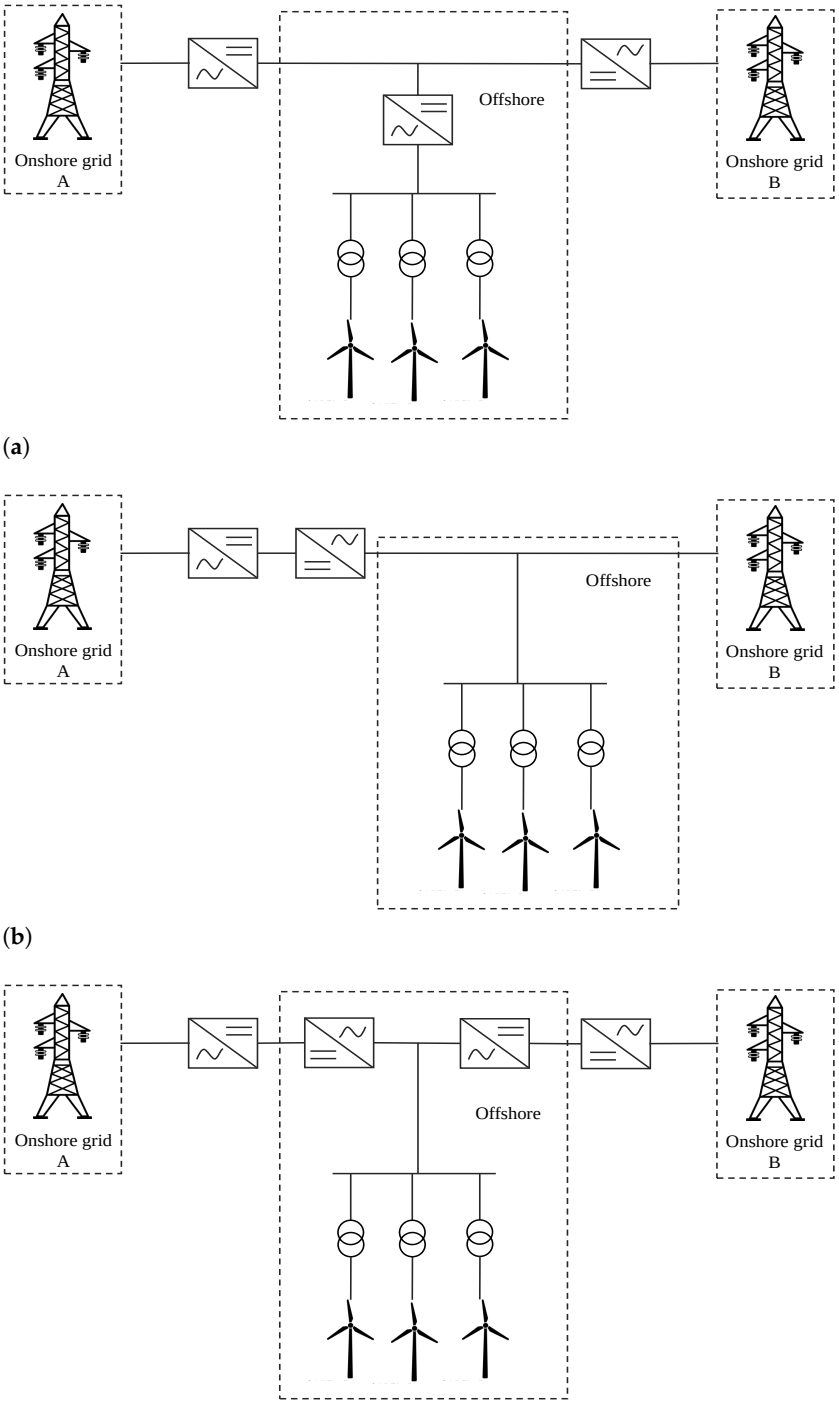

Figure 1. Different configurations available for Hub-and-spoke principle. (**a**) Hub-and-spoke with multi-terminal HVDC system; (**b**) Hub-and-spoke with AC links and HVDC back-to-back station; (**c**) Hub-and-spoke with multiple HVDC links.

The layout of the 2 GW offshore network is built in RSCAD by scaling aggregated OWF model from [12]. A modular topology is considered to achieve the capacity of 2 GW. The following steps are utilized:

- The aggregated OWF model in [12] provides a generation of ∼700 MW. The first step involves reducing this generation to ∼500 MW, because there are four planned OWFs. This is achieved by reducing the number of parallel WG units from 116 (116 × 6 MW = 696 MW) to 83 (83 × 6 MW = 498 MW), which is done by changing the scaling factor

at the OWF transformer. Thus, OWF generates approximately ∼500 MW, as shown in Figure 2.

- The second step involves the connection of two OWFs in parallel to the external AC system in a modular approach. This allows for the generation of 1 GW of power, as depicted in Figure 3. All control structures incorporated in OWF-1 are replicated for OWF-2.
- In the third step, the external AC system is replaced by an offshore converter station, consisting of the average EMT model of MMC (MMC-1) and the interface transformer (IT-1), which is available in the CIGRE B4 DC Grid Test System [14]. The same is depicted in Figure 4. As the final layout network would be extensive, it is required to split the network into subsystems. The splitting into two subsystems is performed in this step. The offshore converter station is modelled in subsystem-1, and the OWFs are modelled in subsystem-2. MMC-1 is designed to operate in V/F control (or grid forming control), which is explained at the end of this section.
- The final step involves parallel connection of the two more OWF models (OWF-3 and OWF-4), generating ∼500 MW each, using modular approach. Additionally, another offshore converter station, consisting of a similar average EMT model of MMC (MMC-2) and two interface transformers (IT-2a and IT-2b), is connected in parallel to the previous converter station. The need for two interface transformers in MMC-2 bus is explained in the following sections of the paper. Therefore, the final layout shown in Figure 5 represents a total of 2 GW offshore wind power transmission.

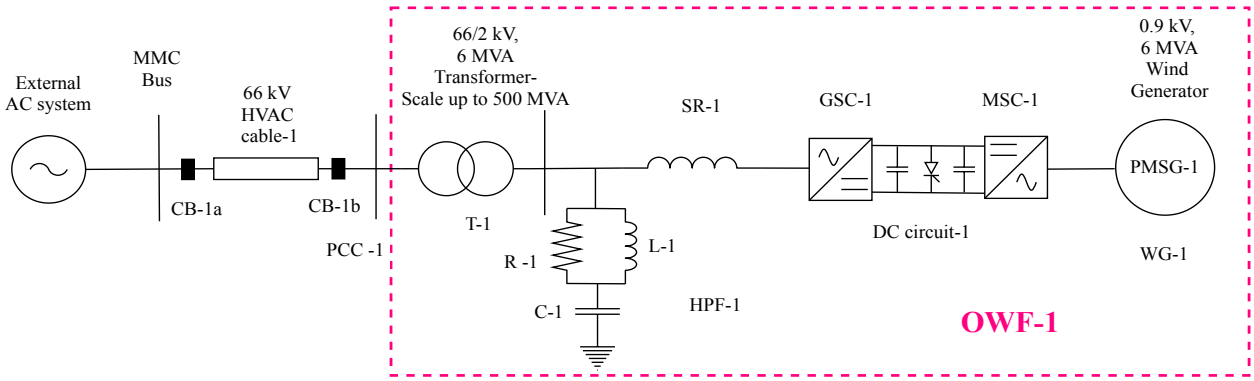

Figure 2. OWF-1 connected to external AC system.

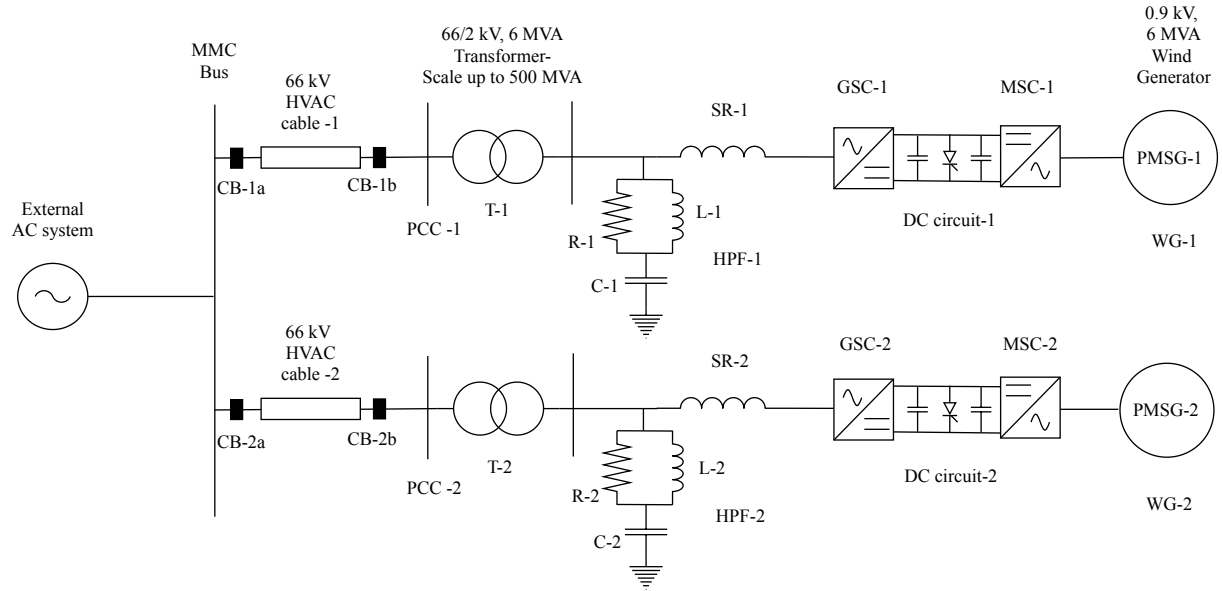

Figure 3. OWF-1 and OWF-2 connected in parallel to external AC system.

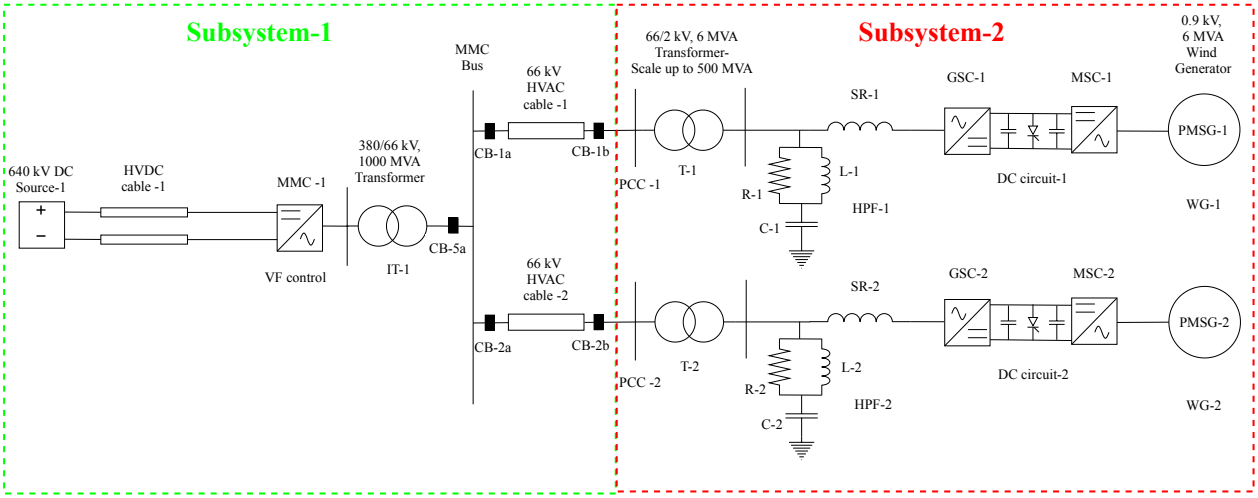

Figure 4. OWF-1 and OWF-2 connected in parallel to MMC-1.

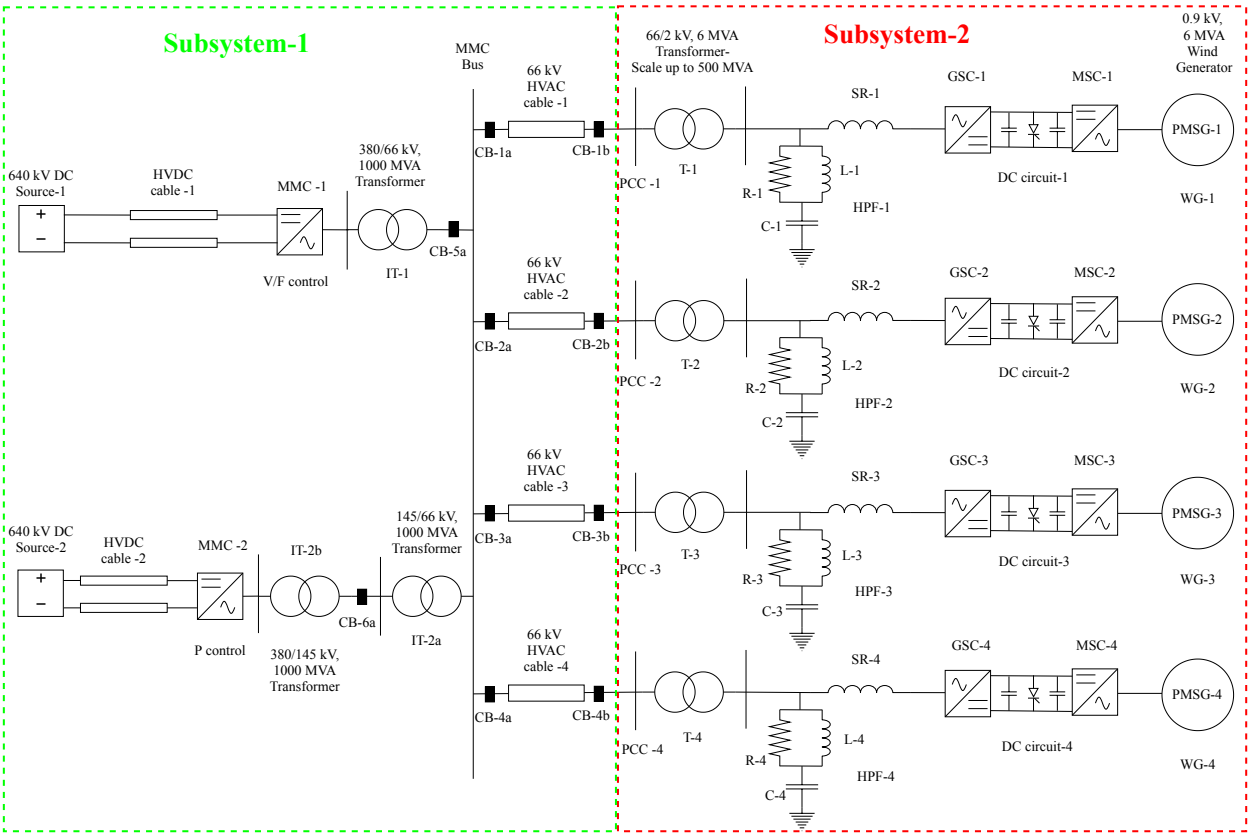

Figure 5. Single line diagram of 2 GW, 66 kV HVAC offshore network connected to 2 × 1 GW HVDC links with offshore converter stations in RSCAD.

3. Layout of 2 GW, 66 kV HVAC Offshore Network in RSCAD

The components used for modelling of 2 GW, 66 kV HVAC network are described in this section. The single line diagram of the network is depicted in Figure 5 and the major components of the network include: four aggregated OWFs (each with 500 MW installed capacity represented by Wind Generation System, High Pass filter (HPF) with series reactor, and OWF transformer), four pairs of HVAC cables, three interface transformers, two MMCs, and two pairs of HVDC cables.

3.1. Aggregated OWF

As mentioned in Section 2.1, the 2 GW offshore wind power is split into four OWFs, with approximately 500 MW rated capacity each. Currently, the largest offshore WG developed by GE Renewable Energy has a rating of 12 MW [15]. The standard model for a Type-4 WG in RSCAD is rated 6 MW. Hence, to represent a 500 MW OWF, 83 WGs are required. All OWFs are at a distance of 30 km from the MMC bus.

The average RSCAD model of Type-4 WG is used. The aggregated OWF model represented in a small time step environment described in [12] is used here for all the four OWFs. As the entire network is extensive, it is split into two subsystems in RSCAD, as shown in Figure 5. The four OWFs are modelled in subsystem-2, and the rest of the system is modelled in subsystem-1. Each subsystem requires one rack for operation, and hence two NovaCor racks are used. It is also possible to simulate the network with PB5 processor. However, this requires three subsystems, since PB5 racks allow only small network simulation [16]. Therefore, two OWFs are to be modelled in subsystem-3, other two OWFs in subsystem-2 and the rest of the network in subsystem-1. Henceforth, the simulations are implemented only on NovaCor processor. Since there is a need for four different small time step blocks which represent four OWFs, each block needs to be set with different step sizes to avoid conflict during initialization. Moreover, if the time steps are not initialized properly, it could lead to the occurrence of a time step overflow error during the simulation in the Runtime module.

Another essential parameter to be considered here is the assignment of the cores for the small time step blocks. NovaCor processor at TU Delft has four cores, and each component used in the network can be assigned to specific core (1 to 4 in number). Since there are six small time step blocks (OWF-1, 2, 3 and 4; MMC-1 and MMC-2), the cores need to be manually assigned to each block to allocate the load on each processor within their capacity. The core allocation of the small time step blocks representing OWFs for this network is chosen, as shown in Table 1.

Table 1. Core assignment of OWF models in subsystem-2.

Small Time Step Block	Core Assignment
OWF-1	4
OWF-2	1
OWF-3	3
OWF-4	1

3.2. HVAC Cables

The HVAC cables transfer power from the OWFs to the offshore converter stations. Hence, four pairs of HVAC cables are required to transfer power from four OWFs. The cables are rated at 66 kV and are 30 km long. In the RSCAD network layout, as shown in Figure 5, the HVAC cables connect OWFs in subsystem-1 with the MMC bus in subsystem-2. To provide connection between components placed in different subsystems in RSCAD, a feature called Tline module is used.

The cables are modelled as Bergeron models with RLC data parameters. Bergeron model is chosen to test the working of the network using travelling wave model. Moreover, as the 2 GW offshore network is developed from the single OWF model in [12], the same RLC cable parameters used in [12] are used in the Tline module for all four pairs of cables.

3.3. Offshore Converter Stations

The offshore converter stations convert HVAC offshore wind power to HVDC to transfer the power to the onshore system through HVDC links. The existing available HVDC links in the industry have a rated capacity of 1.4 GW. Examples of these projects are the NordLink cable connecting Norway and Denmark, NSN Link connecting Norway and the United Kingdom [17]. Moreover, the standard EMT models for MMCs available

in CIGRE B4 DC Grid Test System [14] have a rated capacity of 1.2 GW. Therefore, with the currently available technology, two offshore converter stations are required for the transfer of 2 GW offshore wind power. As MMCs also involve PE components, similar to the OWF model, the average EMT model of MMC is also represented in a small time step environment in RSCAD, in order to represent fast switching events accurately. The average EMT model consists of the MMC and interface transformer modelled in the small time step environment, which represents the offshore converter station. For this work, two small time step blocks are required for the representation of two offshore converter stations. Both blocks are placed in subsystem-1. Again, these two blocks need to be initialized with different time step to avoid conflict during initialization and thereby, avoiding the time step overflow error during the start of simulation. To evenly distribute the load on four cores, considering the core allocation for OWFs in Table 1, the cores for MMCs are allocated as shown in Table 2. The offshore converter station-1 consists of the interface transformer (IT-1) and MMC-1 whereas offshore converter station-2 consists of the interface transformers (IT-2a, IT-2b) and MMC-2.

Table 2. Core assignment of MMC models in subsystem-1.

Small Time Step Block	Core Assignment
MMC-1	3
MMC-2	2

3.3.1. Interface Transformers

Interface transformers (also termed as converter transformers) are connected to the AC side of MMCs and depicted as IT-1 for offshore converter station-1 and IT-2a and IT-2b for offshore converter station-2, see Figure 5. As explained in [18], these transformers provide reactance between the offshore network and the MMC, and prevent the flow of zero sequence currents between the offshore network and the MMC.

As mentioned in Section 3.3, in the available average EMT models in RSCAD library, the interface transformer is modelled with the MMC in a small time step environment. Considering a delta-wye type interface transformer and connecting MMC to the delta side of the transformer, allows isolation of the zero sequence currents during faults. The available EMT models for offshore MMC stations from [14] are utilized in this work. These models are designed for 145 kV HVAC offshore network. Hence, the secondary side voltage of the transformer is changed from 145 kV to 66 kV. Additionally, there were modifications in the control structures of the MMC to make them fitting for the 66 kV HVAC network. Control modifications are explained in the next section.

There are mainly three interface transformers used in this work. The transformer (IT-1) is rated 66/380 kV, 1000 MVA in the offshore converter station-1. Two interface transformers in the offshore converter station-2 are rated 66/145 kV, 1000 MVA (IT-2a) and 145/380 kV, 1000 MVA (IT-2b) respectively. The need for two interface transformers in offshore converter station-2 is explained in the later sections in the paper.

3.3.2. Modular Multilevel Converters (MMCs)

The average EMT model of MMC in RSCAD has the option of modelling the MMC using half-bridge submodules or full-bridge submodules [19]. The voltage levels for HVDC offshore wind farm projects in Europe range from 300 kV to 640 kV DC voltage [17]. Hence, to continue with the latest trend, a voltage level of 640 kV DC is chosen for this work. Therefore, 320 submodules are required per arm to create a voltage of $\pm$320 kV for the positive and negative poles, respectively. Both MMCs (MMC-1 and MMC-2) in the offshore converter stations are modelled for 640 kV DC.

3.4. HVDC Cables

The HVDC cables transfer the generated wind power from the offshore converter station to the onshore system. As mentioned in the section above, the voltage level chosen for HVDC transmission in this work is 640 kV DC. Therefore, each cable model must be suitable for ±320 kV. The cable parameters available in [14] designed for ±400 kV voltage are utilized in this work. The cable model is represented in frequency-dependent phase domain using the Cable module available in RSCAD. The cables are modelled in subsystem-1 and labelled as HVDC cable-1,2 for the connection from offshore converter station-1 and offshore converter station-2 to the onshore system, respectively (see Figure 5).

3.5. Onshore Equivalent Converter Stations

The connection between offshore converter station and the onshore converter station follows a symmetrical monopole configuration, as shown in Figure 6a [20]. The DC part of the onshore converter stations are simplified and represented using an equivalent DC source, as shown in Figure 6b. This simplification is valid, because the paper deals with dynamical performance on the network's AC side. Conventionally, the onshore converter stations provide DC voltage and reactive power control. Hence, the representation of a constant DC voltage source ensures the DC voltage control during the time of disturbances in the AC offshore network. The voltages of the DC sources are 640 kV.

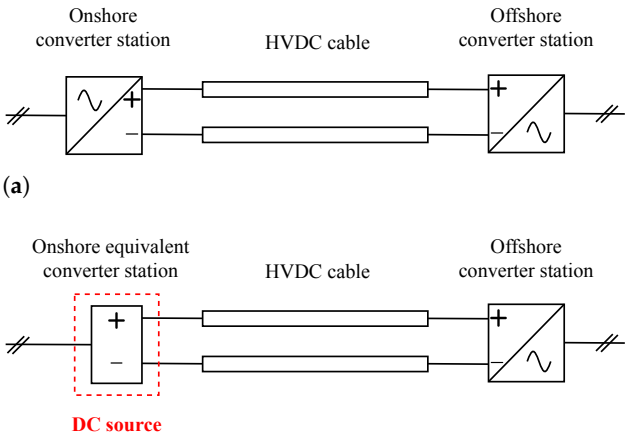

Figure 6. Symmetrical monopole configuration in HVDC network. (**a**) Symmetrical monopole configuration; (**b**) Symmetrical monopole configuration by equivalent representation of DC side of onshore MMC station using a constant DC source.

4. Control Structures

This section explains the different control structures and the modifications required to ensure converters' operation in the 66 kV HVAC network. The DVC from [21] for Type-4 WG, firstly implemented in [12], is extended for the 2 GW offshore network. There are three control strategies used: DVC in the GSCs of the WGs used to represent aggregated OWFs, island mode control in MMC-1, and non- island mode control in MMC-2.

4.1. DVC

The control structure explained in [12] is implemented for all the four WGs. Since the same type of model is used for GSCs in all four WGs, the control loop parameters remain the same.

4.2. Island Mode Control

It is highly necessary to use a control strategy in any of the MMCs which could provide the voltage and frequency reference for the MMC bus since it is connected to a weak network (OWF network). The reference voltage is created by the V/F control mode,

which comes under the classification of the islanded mode of control for VSCs [14]. For this study, MMC-1 is operated in the V/F control. A basic control strategy was developed according to the illustration provided in [22] and it is shown in Figure 7. Since the voltage angle reference (θ) is generated by an independent Voltage Controlled Oscillator (VCO), this control is termed under island mode operation. Such an approach provides the grid forming behaviour for MMC-1, which is responsible for providing and absorbing power from the OWF network when required. With this control the power flow is kept in balance during the steady state and transient conditions [5].

The V/F control consists of a PI controller whose input is the difference between the measured voltage (V_{PCC}) and the reference PCC voltage (V_{PCC_ref}), given in p.u. PI controller provides a reference d-axis converter voltage (V_{PCC_d}) that is translated to abc frame (V_{abc_ref}), as shown in Figure 7. This makes V_{PCC_d} to be aligned with the grid voltage and the q-axis voltage (V_{PCC_q}) is set to zero. The parameters for the PI gains used for this control are referred from [14]. It should be noted that all figures representing control approach have notation in Laplace domain, where s is a Laplace operator.

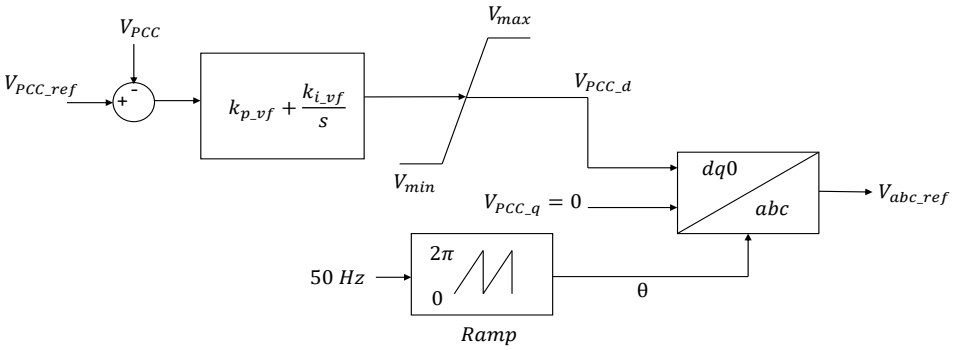

Figure 7. V/F control in MMC-1.

4.3. Non-Island Mode Control

This mode of operation is based on the conventional current control (grid following) approach, which consists of the outer control loop and the inner control loop. The outer loop consists of the direct (d) and quadrature (q) axes loops. The d-axis loop can provide control of DC voltage or active power and the q-axis loop can provide control of an AC voltage or reactive power, as depicted in Figure 8a and Figure 8b, respectively. The outer control loop provides the respective current reference values as inputs for the inner current loops. MMC-2 is configured with this control for this work.

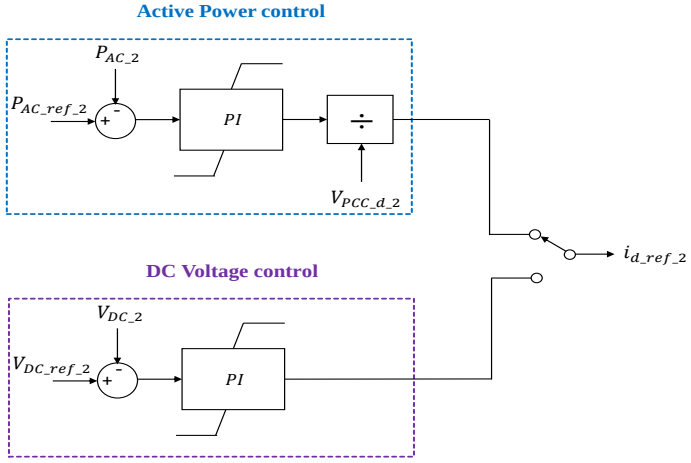

(**a**)

Figure 8. *Cont.*

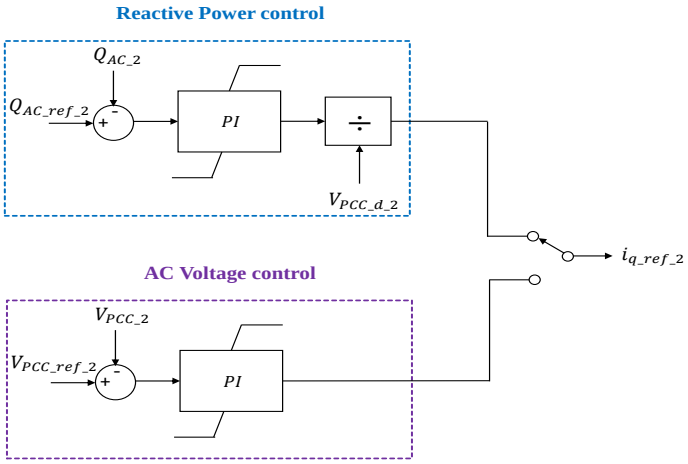

(**b**)

Figure 8. Simplified structure of the outer loop control for MMC-2. (**a**) Outer control loop representation for d-axis ($i_{d\_ref\_2}$); (**b**) Outer control loop representation for q-axis ($i_{q\_ref\_2}$).

The parameters defined in this section are mathematically derived in [23]. The rotating dq frame provides a simplified control for the three-phase systems. The currents and voltages in the abc frame are transformed into dq frame using Clarke-Park transformation. As conventionally followed, the d-axis voltage is aligned with the grid voltage ($V_{PCC\_d\_2}$) at the HV bus of IT-2a interface transformer, and the q-axis is set to zero. This provides constant values for d and q components during steady state.

If active power is the priority in d-axis, active power control of MMC-2 is given by Equations (1) and (2):

$$P_{AC\_2} = V_{PCC\_d\_2} \times i_{d\_2}, \tag{1}$$

$$i_{d\_ref\_2} = \frac{1}{V_{PCC\_d\_2}} \left(k_{p_P} + \frac{k_{i_P}}{s} \right) \left(P_{AC\_ref\_2} - P_{AC\_2} \right). \tag{2}$$

However, if DC voltage is the priority in d-axis, DC voltage control is provided by the following equation:

$$i_{d\_ref\_2} = C_{V_{DC\_2}}(s) \times \left(V_{DC\_ref\_2} - V_{DC\_2} \right), \tag{3}$$

where $C_{V_{DC\_2}}$ is the transfer function of the DC voltage control.

If reactive power is the priority in q-axis, reactive power control of MMC-2 is given by the following equations:

$$Q_{AC\_2} = -V_{PCC\_d\_2} \times i_{q\_2}, \tag{4}$$

$$i_{q\_ref\_2} = -\frac{1}{V_{PCC\_d\_2}} \left(k_{p_Q} + \frac{k_{i_Q}}{s} \right) \left(Q_{AC\_ref\_2} - Q_{AC\_2} \right). \tag{5}$$

The voltage difference at the equivalent reactance interface is calculated as following:

$$\Delta V_{PCC\_2} = V_{conv\_2} - V_{PCC\_2} \approx \frac{\omega (L_{trafo\_2} + L_{arm\_2}/2) Q_{AC\_2}}{V_{PCC\_2}}, \tag{6}$$

where L_{trafo_2} is the interface transformer (IT-2b) leakage reactance and L_{arm_2} is the arm inductance in MMC-2.

Since the d-axis voltage is aligned with the grid voltage, inserting Equation (4) in Equation (6), the following equation is obtained:

$$\Delta V_{PCC\_2} \approx \omega (L_{trafo\_2} + L_{arm\_2}/2) \times i_{q\_2}. \tag{7}$$

The control of AC voltage is obtained with the following equation:

$$i_{q\_ref\_2} = \left(k_{p_V} + \frac{k_{i_V}}{s}\right)\left(V_{PCC\_ref\_2} - V_{PCC\_2}\right). \tag{8}$$

The inner loop consists of PI controllers for d and q axis separately, and it provides a decoupled control action. The output from the inner control loop control is then translated back to the abc frame using dq to abc frame transformation.

As the DC voltage in the HVDC link is maintained and controlled by the onshore equivalent MMC station represented by a constant DC source, the active power control is chosen as priority for d-axis for MMC-2 control. Similarly, as the AC voltage is controlled by the V/F control in MMC-1, reactive power control is chosen as priority chosen for q-axis for MMC-2. When active power is the chosen priority, $P_{AC\_ref\_2}$ represents the required amount of active power that must flow through offshore converter station-2 and must be defined externally by the user. However, the outer loop control available for the non-islanded mode in [14] is not suitable for parallel operation with V/F control. Hence, the outer loop is simplified, and the reference points $i_{d\_ref\_2}$ and $i_{q\_ref\_2}$ for the inner loop are controlled directly by the user. The inner control loop consists of PI controllers that play the major role in ensuring minimum steady state error. The inner control also contains the feed-forward term to compensate the cross coupling terms. The mathematical equations for the parameters of inner control loop are derived as provided in [23]. Applying Kirchoff's Voltage Law in Figure 9 and with the MMC representation in Figure 10, the equations are derived for offshore converter station-2 connected to the AC network. The assumptions involve, the direction of current is from the AC network to the MMC (the condition when offshore wind power is transferred from the offshore network to onshore system) and avoiding the star-point reactor:

$$\frac{V_{DC\_2}}{2} = v_{uj} + L_{arm\_2}\frac{di_{uj}}{dt} + R_{arm\_2}i_{uj} - L_{trafo\_2}\frac{di_j}{dt} - R_{trafo\_2}i_j + v_{PCC_j}, \tag{9}$$

$$\frac{V_{DC\_2}}{2} = v_{lj} + L_{arm\_2}\frac{di_{lj}}{dt} + R_{arm\_2}i_{lj} + L_{trafo\_2}\frac{di_j}{dt} + R_{trafo\_2}i_j - v_{PCC_j}, \tag{10}$$

where R_{trafo_2} is the interface transformer (IT-2b) resistance, R_{arm_2} is the equivalent arm resistance in MMC-2, v_{PCC_j} is the voltage at HV bus of IT-2a, $j \in \{a, b, c\}$ represents phases. Upper arm and lower arm of the MMC-2 are denoted as u and l, respectively.

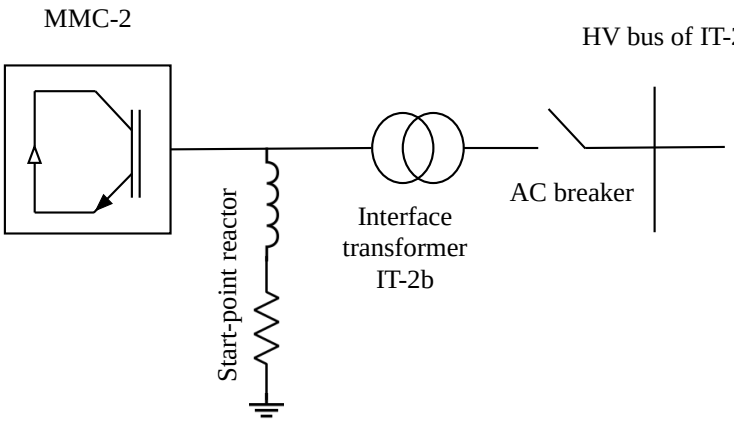

Figure 9. Representation of offshore converter station-2 connection to the AC offshore network.

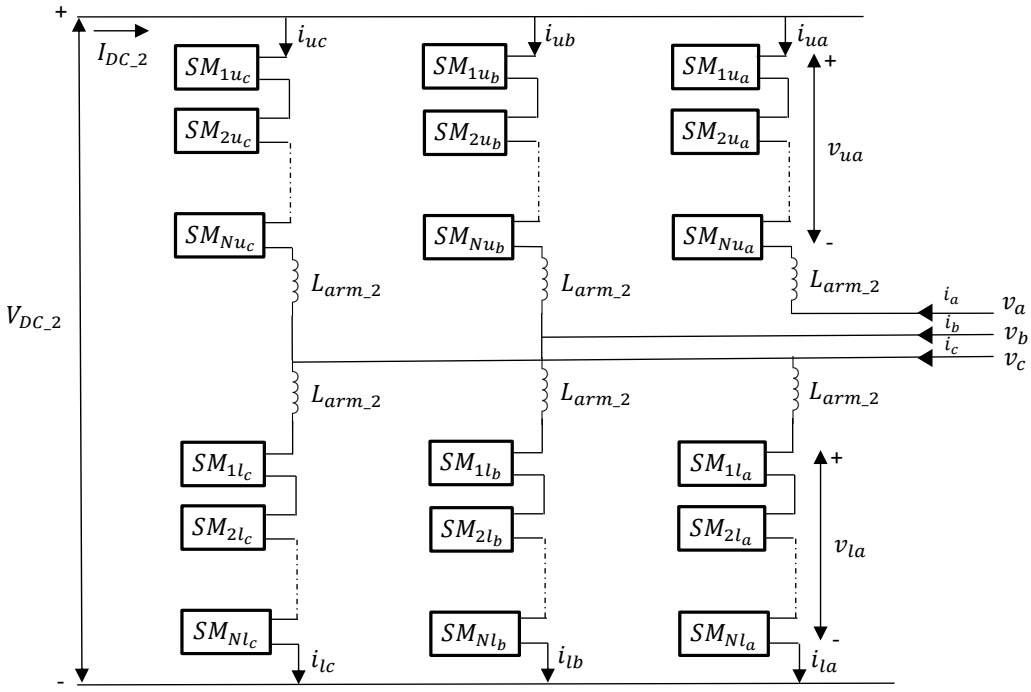

Figure 10. MMC-2 representation.

The equations in dq frame can be represented as follows:

$$V_{PCC\_d\_2} - V_{conv\_d\_2} = \left(\frac{L_{arm\_2}}{2} + L_{trafo\_2}\right)\frac{di_d}{dt} + \left(\frac{R_{arm\_2}}{2} + R_{trafo\_2}\right)i_d - \omega\left(\frac{L_{arm\_2}}{2} + L_{trafo\_2}\right)i_q, \quad (11)$$

$$V_{PCC\_q\_2} - V_{conv\_q\_2} = \left(\frac{L_{arm\_2}}{2} + L_{trafo\_2}\right)\frac{di_q}{dt} + \left(\frac{R_{arm\_2}}{2} + R_{trafo\_2}\right)i_q + \omega\left(\frac{L_{arm\_2}}{2} + L_{trafo\_2}\right)i_d. \quad (12)$$

The control loop is defined as follows:

$$V_{conv\_ref\_d\_2} = -\left(i_{d\_ref\_2} - i_d\right)C_{i_{ac}}(s) + V_{PCC\_d\_2} + \omega\left(\frac{L_{arm\_2}}{2} + L_{trafo\_2}\right)i_q, \quad (13)$$

$$V_{conv\_ref\_q\_2} = -\left(i_{q\_ref\_2} - i_q\right)C_{i_{ac}}(s) + V_{PCC\_q\_2} + \omega\left(\frac{L_{arm\_2}}{2} - L_{trafo\_2}\right)i_d, \quad (14)$$

where $C_{i_{ac}}(s)$ is the transfer function of the PI controller.

The inner control loop provides the control of the reference voltages, as depicted in Figure 11, which are then used as inputs for the lower level control.

The inner control loop model available in [14] is only suitable for a 145 kV HVAC network. This is why a second interface transformer (IT-2a) is used to convert the 66 kV HVAC voltage to 145 kV, as shown in Figure 5. To mitigate the effect of this transformer in terms of an impedance, the leakage reactance and the resistance of the transformer are kept minimal (0.001 p.u.). However, it should be noted that this is a simplification used in this work, and such a transformer with very low reactance is not practically used in a power system network. The non-island mode control in MMC-2 identifies the frequency and phase angle at the HV bus of the interface transformer (IT-2a) in Figure 5. The PLL in MMC-2 control performs this task and synchronizes with the measured grid voltage at the HV bus of IT-2a. The PI gains for the PLL were set based on parameter sensitivity analysis. The phase angle is generated by the PLL, which is used to transform it from abc to dq frame.

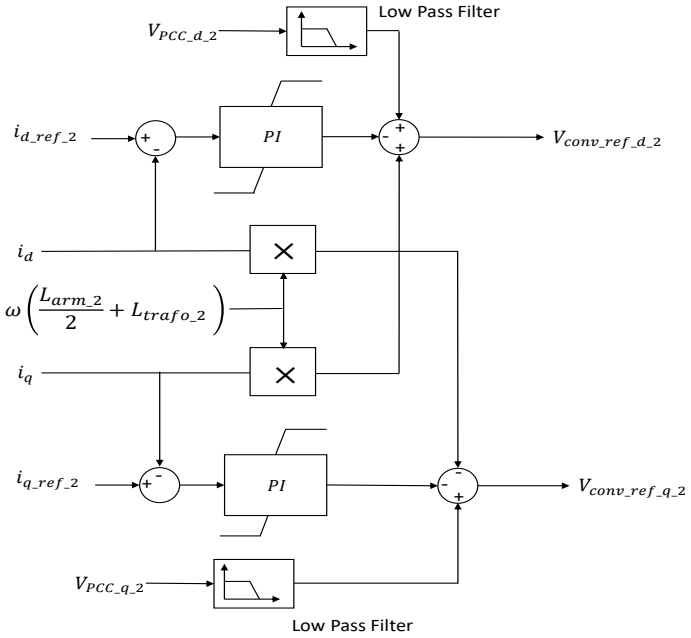

Figure 11. Inner loop control for MMC-2.

The lower level controls such as circulating current suppression control, modulation and third harmonic injection are available in the average EMT model of MMC controls in [14]. They are used in both MMC-1 and MMC-2. Further, the performance of the 2 GW offshore network needs to be analyzed during steady state and dynamic conditions after incorporating the aforementioned control strategies. Therefore, two most severe dynamic scenarios are studied, as depicted in Figure 12, in the following section.

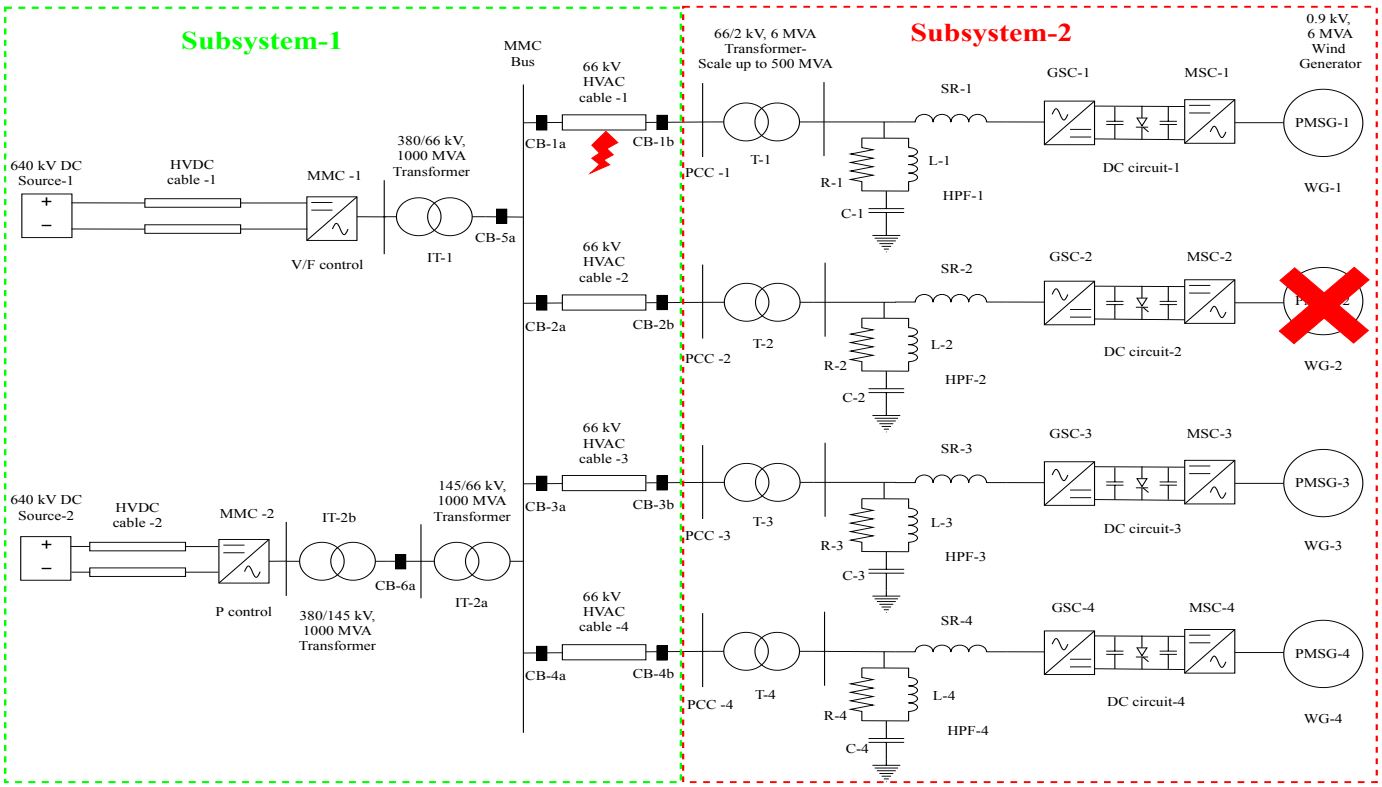

Figure 12. 66 kV HVAC offshore network connected to 2 × 1 GW HVDC links with offshore converter stations in RSCAD for two dynamic scenarios: Disconnection of OWF-2 (represented by the cross symbol); Three-phase line to ground fault in the middle of cable-1 (represented by the fault symbol).

5. Numerical Simulations in RSCAD

5.1. General Settings, Control Modes and Pre-Set Conditions

The simulation time step for all the simulations is set to 50 µs. All plots are simulated for a time span of 5 s. Faults or switching events are timed to occur at 0.5 s of the simulation. The three-phase voltage and current graphs for all simulations are plotted for a shorter period (0.4 s to 1.3 s) to have a clearer view of the signals during the occurrence of an event. However, the voltage in p.u., active and reactive power graphs are plotted for the whole time (5 s) to analyze the voltage stability and power flow in the network during the simulation. In order to analyze the dynamic and steady state operation of the network, the controllers and set points need to be initialized before charging. They are set as follows:

- MMC-1:
  - Islanded mode operation (V/F control)
  - AC voltage control, V_{PCC_ref} = 1 p.u. (Reference AC voltage)
- MMC-2:
  - Non-islanded mode operation
  - Active power control, $I_{d\_ref\_2}$ = 0 (No power flow through MMC-2 in the initial conditions)
- Network:
  - Circuit breakers (CB-1a, CB-1b, CB-2a, CB-2b, CB-3a, CB-3b, CB-4a, CB-4b, CB-5a and CB-6a) in open condition

5.2. Synchronization of the Offshore Converter Stations

The AC side of MMCs need to be connected to simulate the synchronization scenario. Since the DC side is connected to DC sources, the charging of HVDC cables is not considered for this study. As mentioned in Section 4, MMC-1 works as grid forming (V/F control) and MMC-2 works as grid following (active power control). Once the simulation is started, the network is charged through the interface transformer, IT-1. The measurements of voltages, currents and powers for the offshore converter stations are done at the LV side of IT-1 for converter station-1 and LV side of IT-2a for converter station-2. At the points of measurement, the voltages are the same, because they are connected to the same potential (connected to MMC bus). Firstly, the circuit breaker, CB-5a is closed and the MMC bus is charged. The MMC bus voltage builds up to nearly 0.98 p.u. as shown in Figure 13. The currents at the measurement points for both MMCs also increase and settle, as it is shown in Figures 14a,b. The current takes nearly 0.35 s to settle after breaker's closing due to selected PI parameters of the V/F control in MMC-1. Additionally, the transformer IT-2a is also charged in this process.

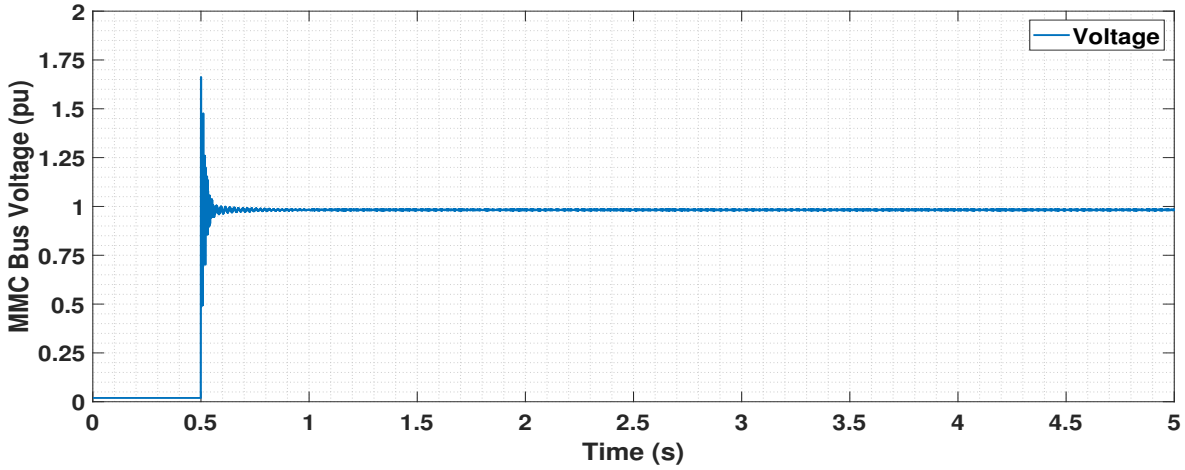

Figure 13. Voltage in p.u. at MMC bus upon CB-5a closing operation.

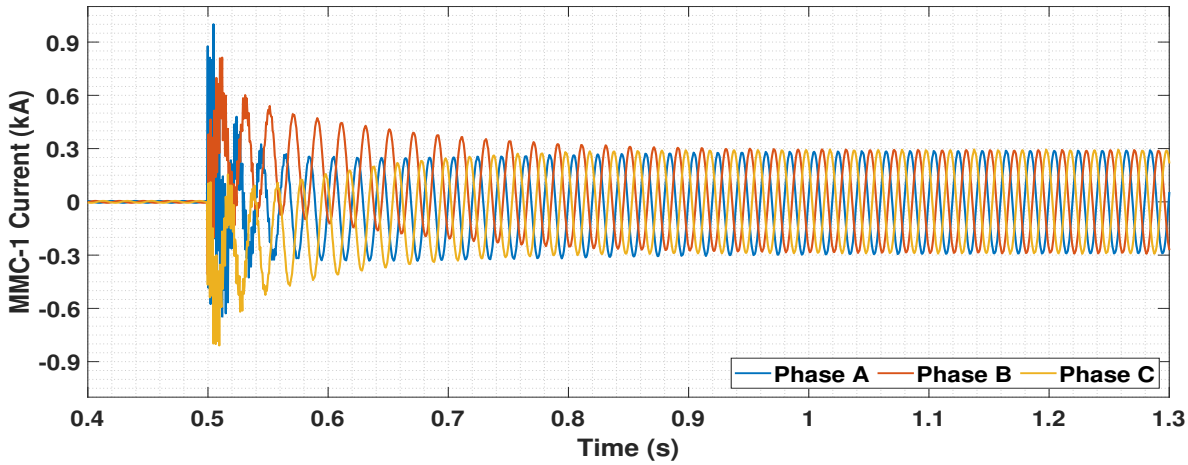

(**a**) Currents in MMC-1 bus

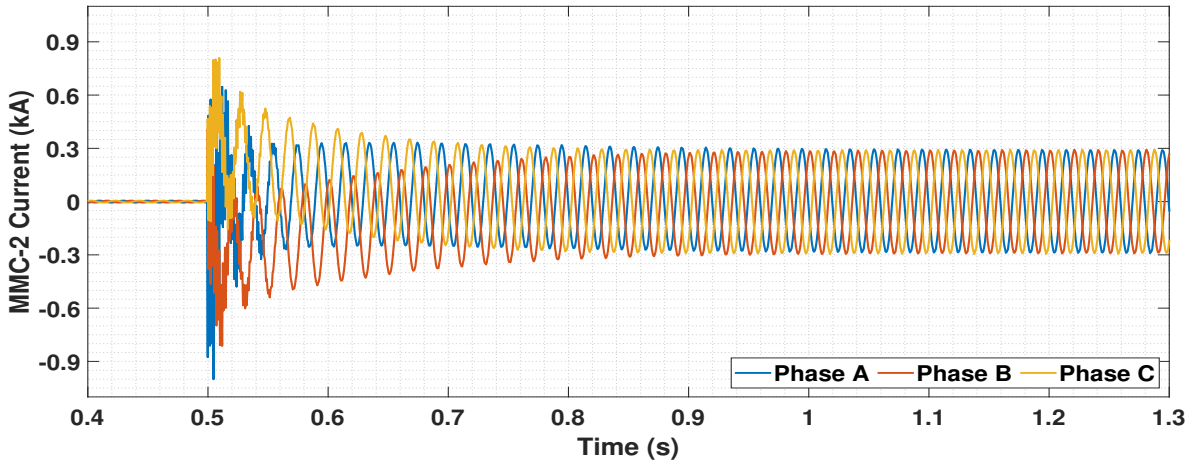

(**b**) Currents in MMC-2 bus

Figure 14. Currents in (**a**) MMC-1 bus and (**b**) MMC-2 bus upon CB-5a closing operation.

The next step is to close the circuit breaker, CB-6a to connect MMC-2 to the network and hence, synchronize it with MMC-1. The voltage at the MMC bus remains the same after connecting MMC-2, as shown in Figure 15. Reason for that is the voltage reference provided and maintained by MMC-1.

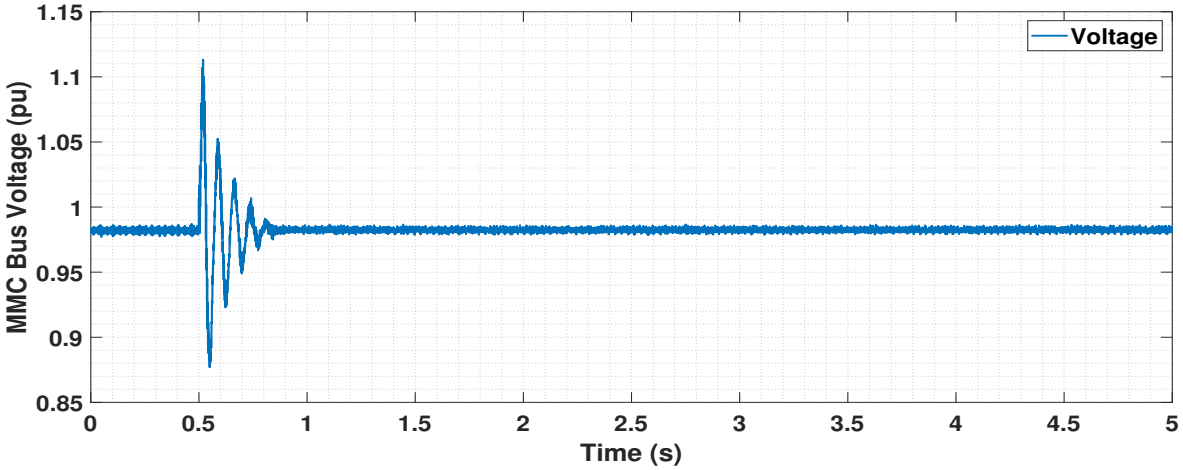

Figure 15. Voltage in p.u. at MMC bus upon CB-6a closing operation.

The currents also remain the same in both MMCs after connection of MMC-2, see Figure 16a,b.

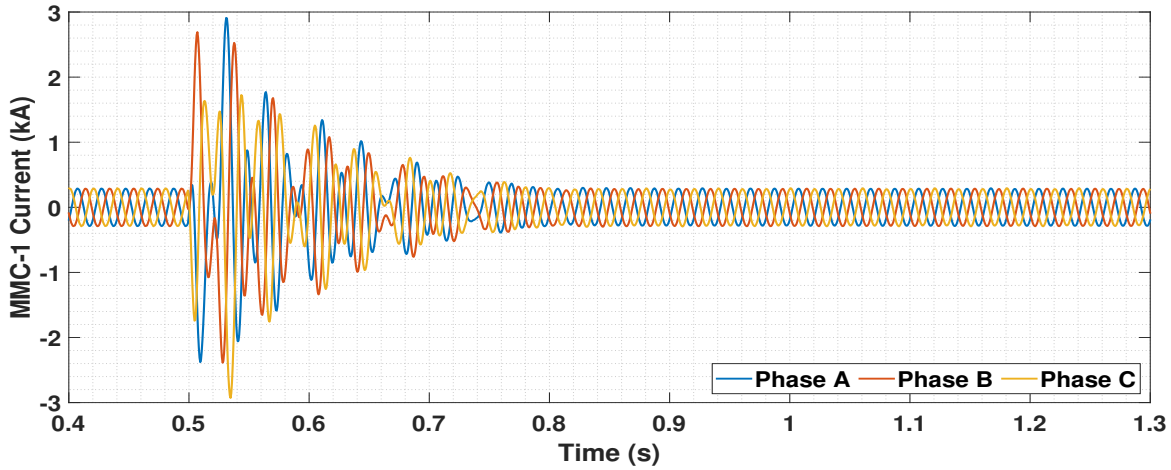

(**a**) Currents in MMC-1 bus

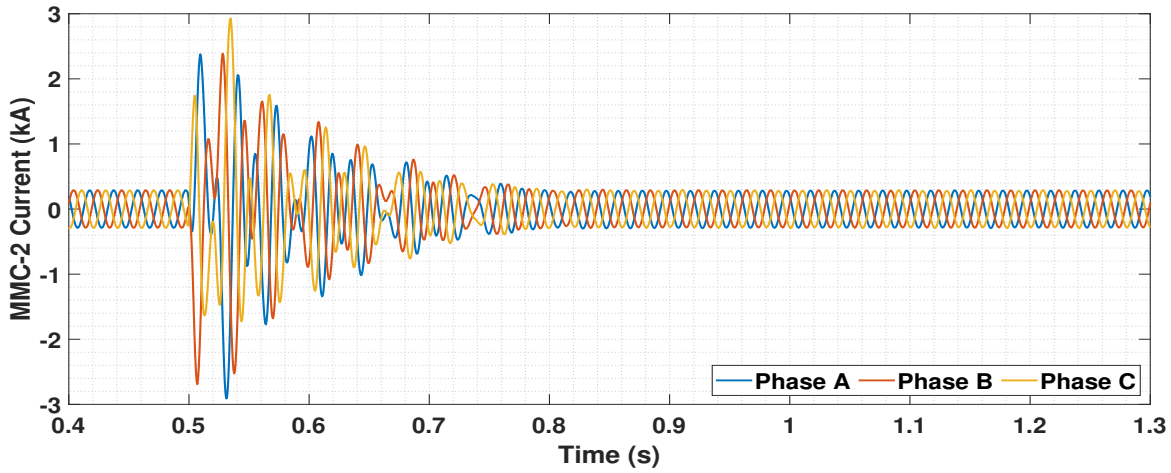

(**b**) Currents in MMC-2 bus

Figure 16. Currents in (**a**) MMC-1 bus and (**b**) MMC-2 bus upon CB-6a closing operation.

5.3. Energization of the HVAC Cables and OWFs

The energization procedure of the AC network, that is followed in this work, involves charging of each HVAC cable and the corresponding OWF. Initially, cable-1 is charged and then OWF-1 is connected. The same is followed for the other OWFs. As mentioned in Section 3.1, each OWF has a maximum capacity of ∼500 MW that is represented by scaling up (by using the scaling factor function in RSCAD) of a WG model with 6 MW rated power. For the energization process, the OWFs are connected initially with lesser number of WG units of ∼50 MW (8 × 6 MW = 48 MW) power to avoid a surge of voltage at PCC and to maintain the voltage within limits. Once stability is attained after connecting all OWFs, the scaling in all OWFs is incremented. Since power only flows through MMC-1, the increment is limited with maximum capacity of MMC-1, i.e., 1 GW.

Cable-1 gets energized when the CB-1a circuit breaker is switched on, as shown in Figure 12. The voltage at MMC bus is increased and set to a value of nearly 1.05 p.u. as seen in Figure 17. MMC-1 provides the current for cable charging and the active power reference for the MMC-2 is not changed in this process. Hence, current flow in MMC-1 bus increases for cable-1 charging as shown in Figure 18a, and the current flow in MMC-2 bus remains unchanged as shown in Figure 18b. The disturbances observed during the

switching operation at 0.5 s occur due to the PI parameters chosen for the V/F control in MMC-1. The current in cable-1 upon CB-1a closing is depicted in Figure 19.

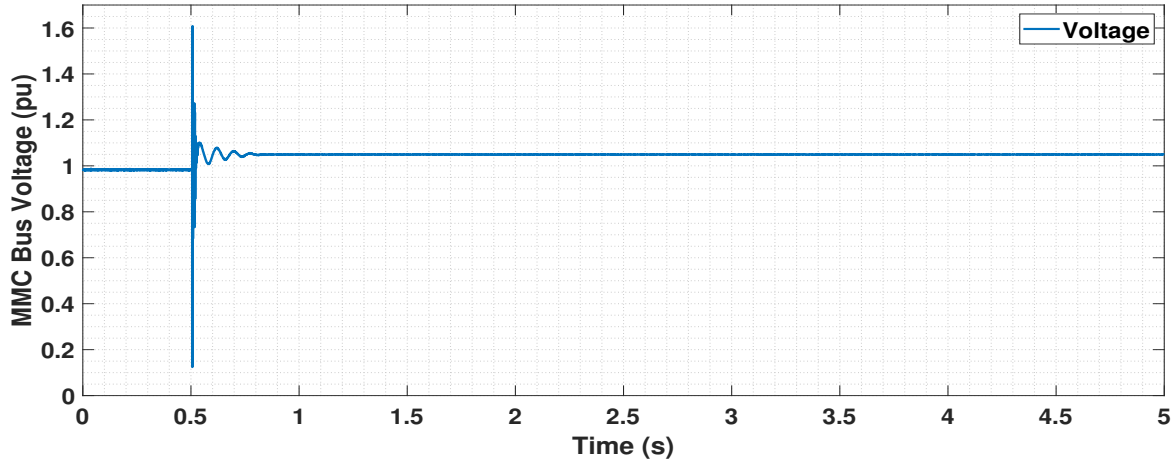

Figure 17. Voltage at MMC bus upon charging of cable-1.

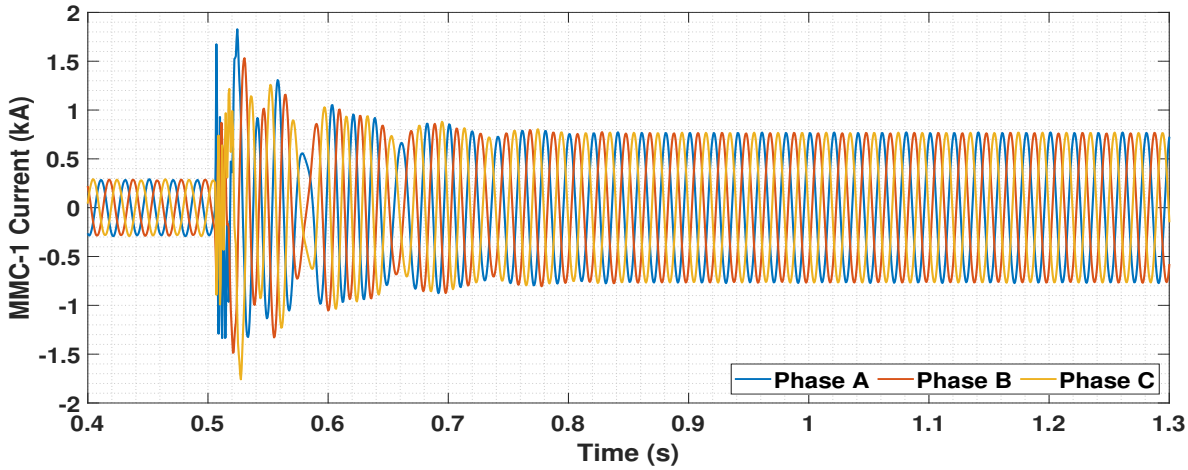

(**a**) Currents in MMC-1 bus

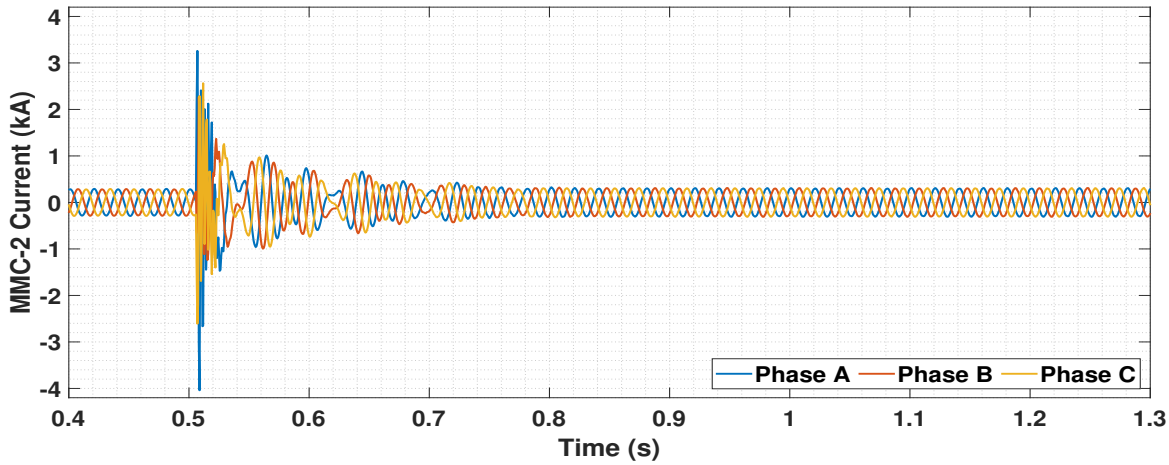

(**b**) Currents in MMC-2 bus

Figure 18. Currents in (**a**) MMC-1 bus (**b**) MMC-2 bus upon CB-1a closing operation for charging of cable-1.

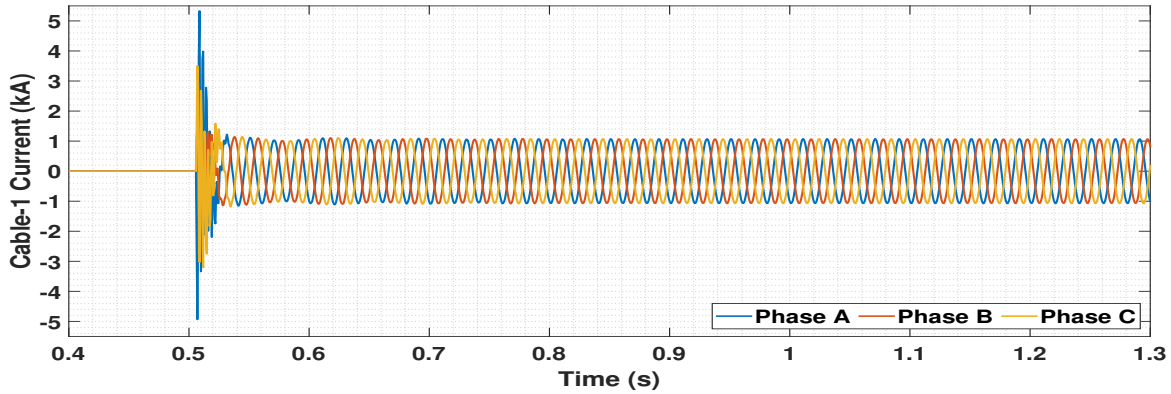

Figure 19. Currents in cable-1 upon CB-1a closing operation for charging of cable-1.

After cable-1 has been charged, the breaker at the OWF-1 end (CB-1b) is switched on. OWF-1 gets connected to the network. As mentioned in Section 5.3, the OWF-1 is connected initially with less generation to keep the voltage at PCC-1 within limits. The initial high voltage at the PCC-1 before closing the breaker, as seen in Figure 20, is due to the capacitance at the DC link. Once the breaker is closed, the voltage is maintained at nearly 1 p.u. as shown in Figure 20. The currents through PCC-1 also increase as shown in Figure 21. The OWF starts generating ∼50 MW, which flows through MMC-1 as shown in Figure 22. In a similar way all other OWFs are connected. All OWFs are connected with ∼50 MW generation. A total power of ∼200 MW through MMC-1 after connection of OWF-1, OWF-2, OWF-3 and OWF-4 is clearly depicted in Figure 22. There is no flow of active power in MMC-2 (Figure 23) since the rated capacity of 1 GW of MMC-1 is yet to be reached.

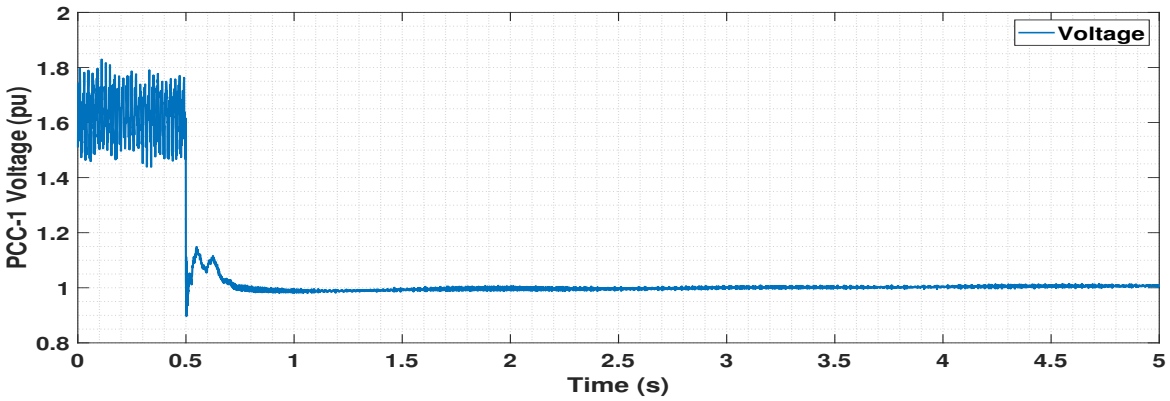

Figure 20. Voltage in p.u. at PCC-1 upon connecting OWF-1 with 50 MW generation to the network.

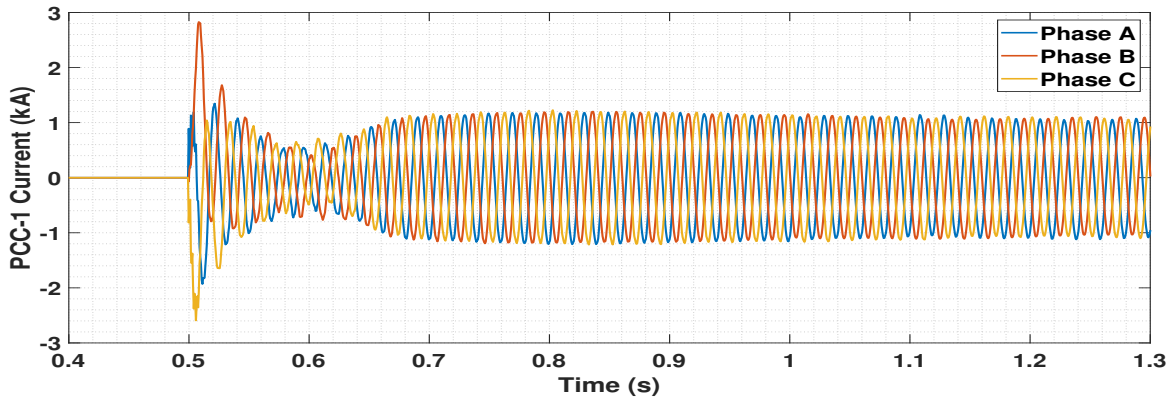

Figure 21. Currents in PCC-1 upon connecting OWF-1 with 50 MW generation to the network.

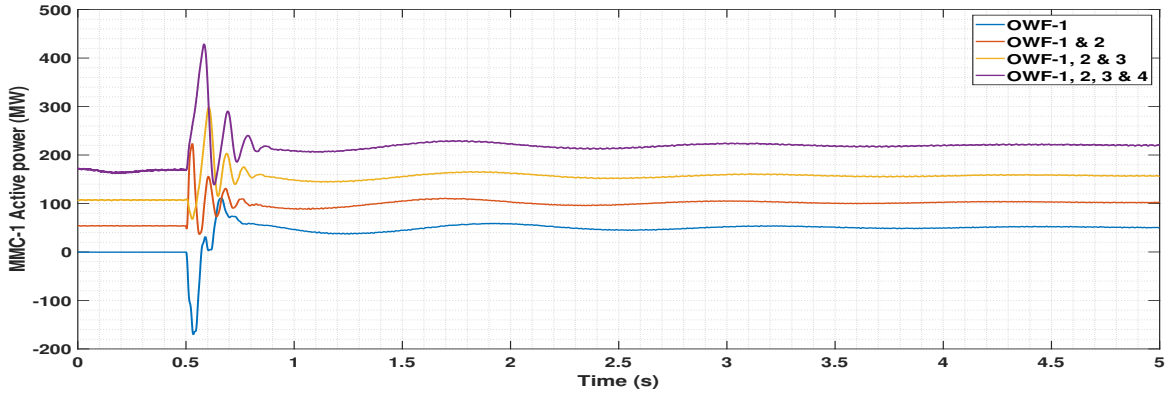

Figure 22. Active power in MMC-1 bus upon connecting all OWFs with 50 MW generation each.

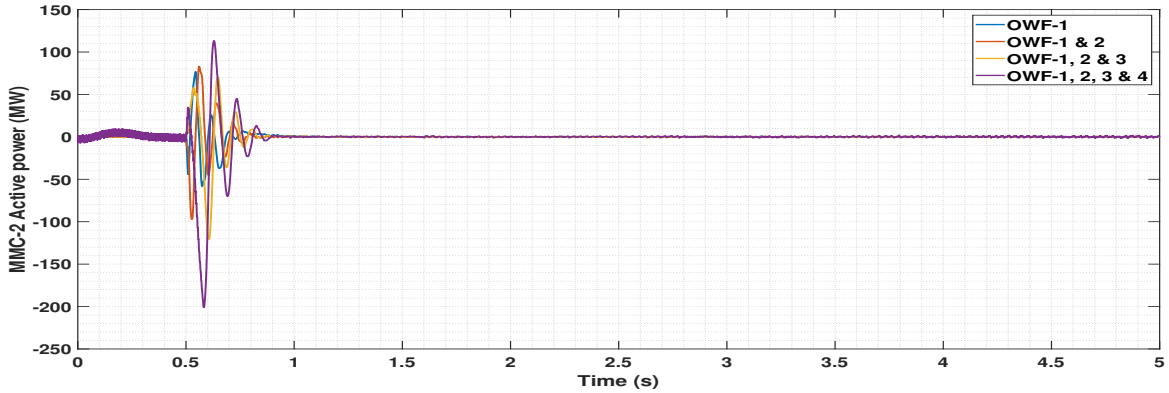

Figure 23. Active power in MMC-2 bus upon connecting all OWFs with 50 MW generation each.

Once the system gets stabilized, the generation is increased in steps, by increasing the number of parallel WG units. Such procedure ensures the voltage to be within limits at all PCCs. The power flow to the MMC-2 has to be controlled in the next step. This is done by controlling the active power reference of the MMC-2. For this study, OWFs are modelled to have the same scaling of power, and hence generate the same amount of power. A step-by-step increment of ∼50 MW in all OWF is done, and correspondingly the active power reference for MMC-2 is also increased. Finally, the OWFs are made to generate ∼500 MW each and the total of nearly 2 GW power is equally split between MMC-1 and MMC-2. Power losses are expected to occur during the transmission, and the active power is nearly 960 MW in both MMCs as seen from the final steady state plots (Figure 24).

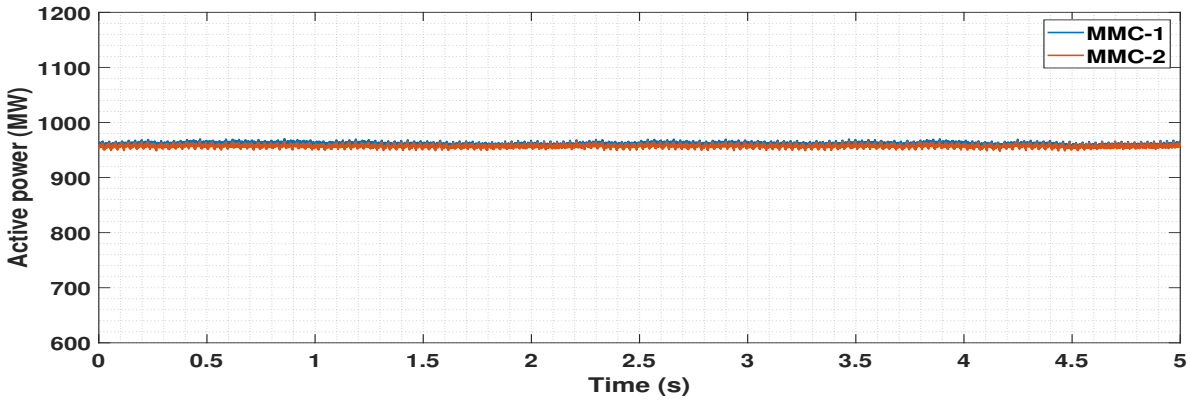

Figure 24. Active power in MMC-1 and MMC-2 buses upon connecting all OWFs with 500 MW generation each.

In Figures 13–24, it can be seen on the respective voltages, currents and powers, that the synchronization of both MMCs, and the energization of the offshore AC grid are done successfully. The offshore AC grid converters and cables now operate at a voltage of 66 kV, the HVDC voltage is set to 640 kV and the total active power is nearly 2 GW. Frequency of the system is stabilized at 50 Hz, and the power system operates in the steady state.

5.4. Dynamic Performance Analysis

Faults and perturbations can occur in the grid, and the components in the system must be able to withstand these voltage surges and fault currents for a short duration of time. The performance of the network in terms of short-term voltage stability (fault occurring for a span of 6–10 cycles accounting for 120–200 ms) and power flow is analyzed. The coordination among different controllers available in the network is studied during severe perturbations.

5.4.1. Disconnection of One OWF

The first event is a sudden disconnection of one OWF. OWF-2 is permanently disconnected from the circuit by opening the breaker, CB-2a connected towards the OWF-2 cable end at the time instance 0.5 s. Once the breaker is opened, the generation of ∼500 MW is lost, and the power flow is reduced through MMC-1, as shown in Figure 25. This is because the MMC-1 is the one in grid forming control (provides power balance in the network), and also because active power reference of MMC-2 is unchanged. In the post-fault period, the active power flow through MMC-2 is seen to be higher than in the pre-fault period. Reason for this can be the increase in voltage at the OWF side. MMC-2 is seen to be operating with the maximum rated capacity of 1 GW in this condition. The decrease in generation in MMC-1 can also be viewed from the currents flowing in MMC-1 as witnessed in Figure 26a, whereas the currents remain the same in MMC-2, as seen from the current in Figure 26b.

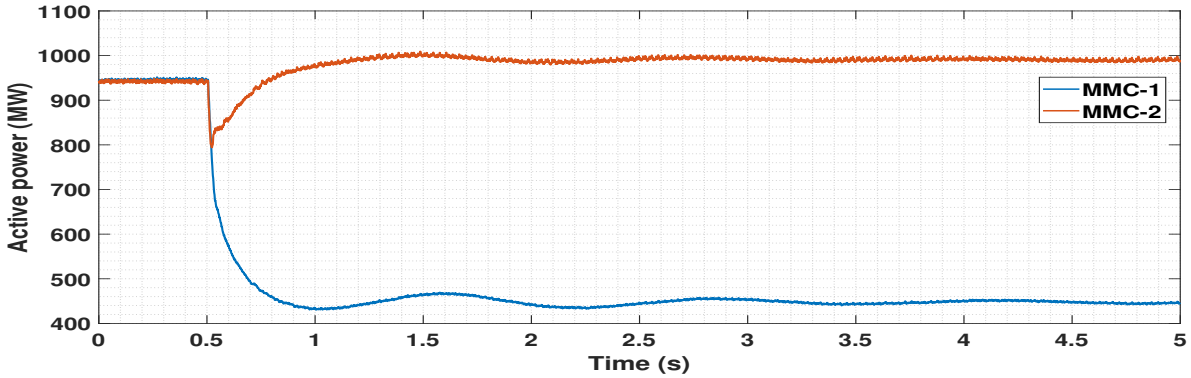

Figure 25. Active power in MMC-1 and MMC-2 buses upon OWF-2 disconnection event.

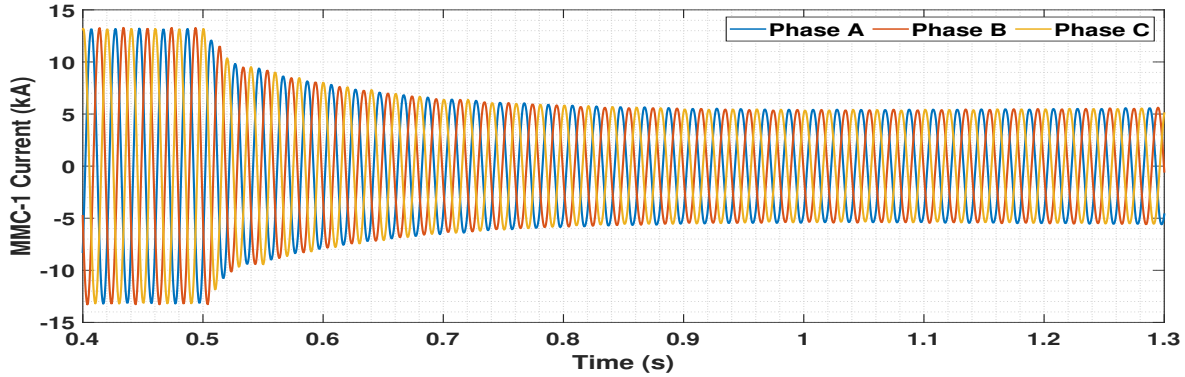

(**a**) Currents in MMC-1 bus

Figure 26. *Cont.*

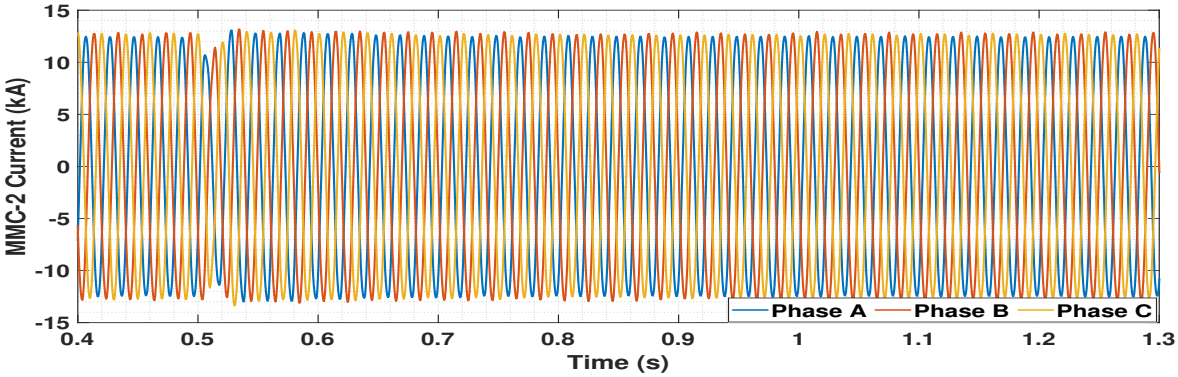

(**b**) Currents in MMC-2 bus

Figure 26. Currents in (**a**) MMC-1 bus and (**b**) MMC-2 bus upon OWF-2 disconnection event.

On the OWFs side, the voltage at PCC-2 goes beyond bounds and it has the same value as before energizing. This can be observed from the voltage in p.u. graph in Figure 27. During the disconnection of OWF-2, occurs a drop in voltages at PCC-1, 3 and 4. This is depicted in Figure 28. It happens since they are all connected to a common bus (MMC bus). Moreover, in the post-fault period, voltages at PCC-1, 3 and 4 are stabilized and settle to a higher value (nearly 1.08 p.u.) than the pre-fault voltage in order to compensate for the loss of OWF-2. This is due to the fast local voltage control in the DVC loop of the WGs. But the currents at these OWFs remain the same since the scaling factor for each OWF is still 83 (83 $\times$ 6 MW = 498 MW). This can be viewed from the current measured at PCC-1 in Figure 29. As voltage increases and current remains the same, the active power generated from the OWF-1, 3 and 4 increases and therefore the power flowing through MMC-2 also increases.

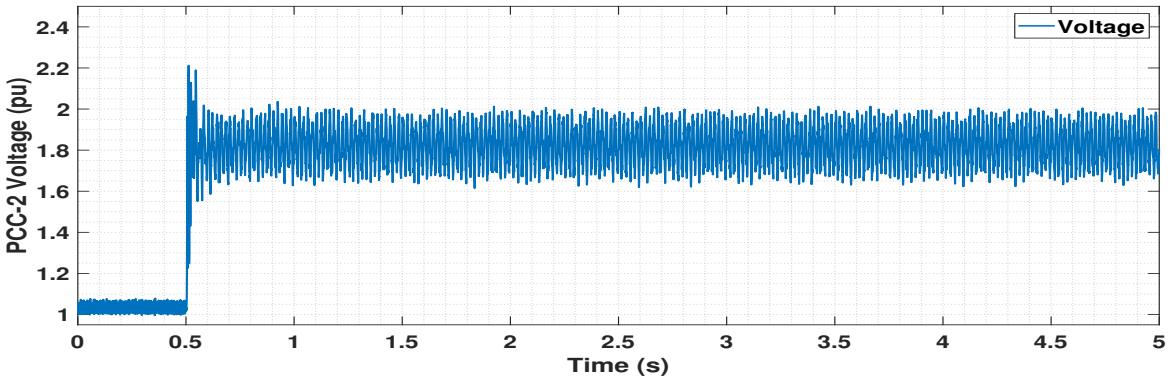

Figure 27. Voltage in p.u. at PCC-2 upon OWF-2 disconnection event.

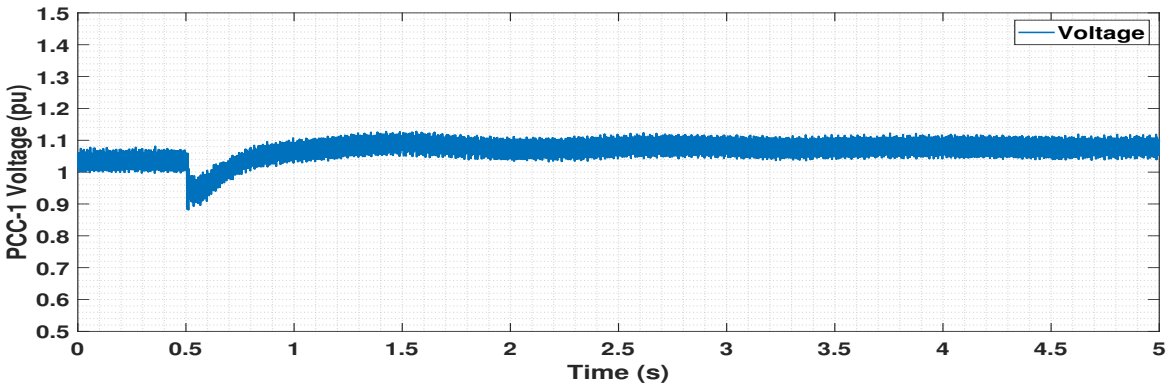

Figure 28. Voltage in p.u. at PCC-1 upon OWF-2 disconnection event.

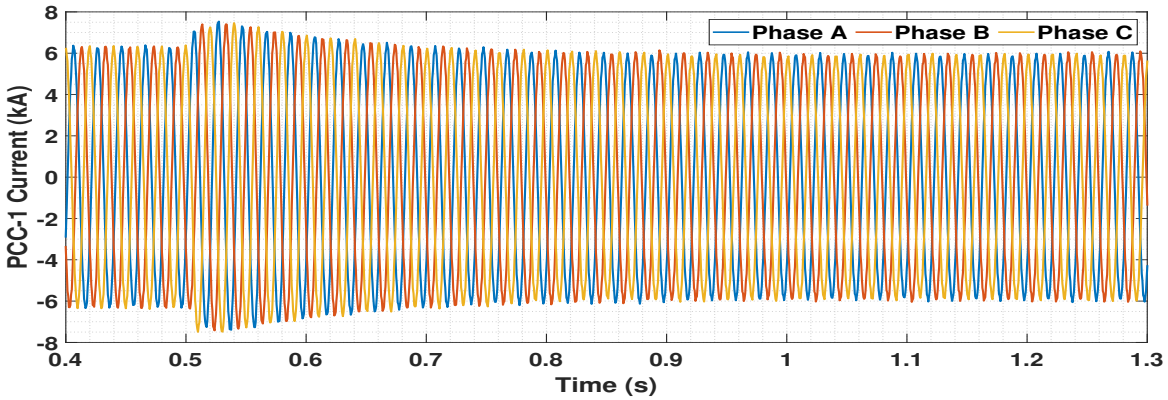

Figure 29. Currents at PCC-1 upon OWF-2 disconnection event.

5.4.2. Circuit Breaker Operation Logic

Before the application of three-phase line to ground fault, a logic to operate the circuit breaker (CB-1a) at the cable-1 end is developed as shown in Figure 30. For the fault, the line to ground fault component available in RSCAD library is used [24].

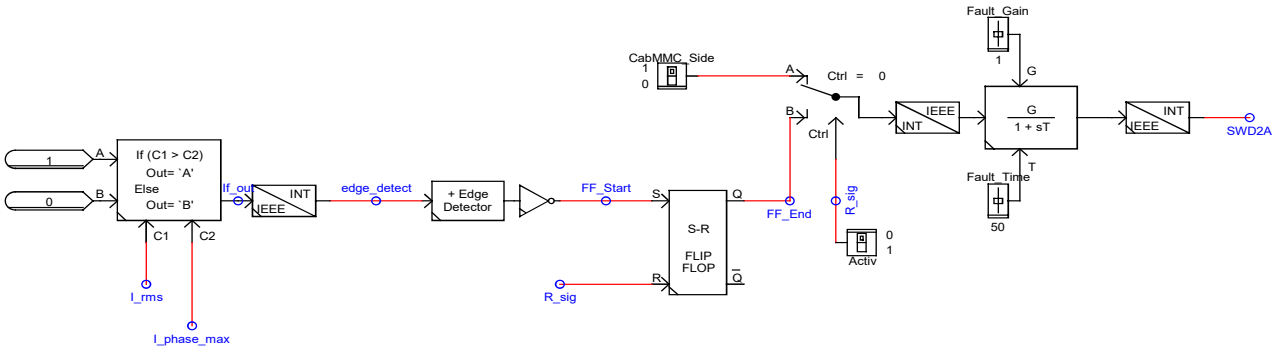

Figure 30. Circuit breaker operation logic

The logic is developed for the operation of the circuit breaker CB-1a in Figure 12 by detecting overcurrent. The signal 'SWD2A' is the signal for operating CB-1a. Initially, the breaker is closed during the energizing process using the switch 'CabMMC_side'. Once the system is fully operational after connecting all four OWFs and achieving 2 GW power in the network, the 'Activ' switch in Figure 30 is turned on. This is done to provide the switching operation of CB-1a by comparing the RMS current I_{rms}, and the maximum phase current I_{phase_max} (I_{phase_max} = 10% above I_{phase} = 1.1 × I_{phase}; $I_{phase} = \frac{Apparent\ \ power\ \ in\ \ single-phase}{Line\ \ to\ \ neutral\ \ voltage}$) at CB-1a. The system is still in steady state condition. Once the fault is applied, when I_{rms} becomes greater than I_{phase_max}, the SR flip flop detects the change and holds a zero value for the signal 'SWD2A'. This action causes the breaker CB-1a to open. The delay block before the signal 'SWD2A' provides time delay for the operation of circuit breaker after the fault has been detected.

In order to analyze the short-term voltage stability of the system, a permanent three-phase line to ground fault is applied in the middle of HVAC cable-1. The response of the network is recorded, and the plots for voltages, currents, active and reactive powers are depicted in Figures 31–39 for the event. During the time of the fault, the RMS current exceeds the maximum phase current and the logic developed detects this overcurrent at CB-1a. This leads to the opening of breaker CB-1a according to the logic explained in the previous paragraph. The overcurrent is detected at 0.53 s of the simulation from the developed logic. A short delay of nearly 12 ms is provided to open the breaker after the fault has been detected similar to a practical scenario (Figure 31). After the circuit breaker is opened, OWF-1 is isolated from the network and total power provided to the onshore

system is reduced. The total power in the pre-fault period is nearly 2 GW, and after the fault, the total power is reduced to nearly 1500 MW. Similarly to the disconnection of one OWF, discussed earlier in Section 5.4.1, the power flow is reduced through MMC-1 as shown by the blue line in Figure 32. It is worth of mentioning that the network is stable by viewing the stable voltage in the post-fault period in MMC bus, as shown in Figure 33.

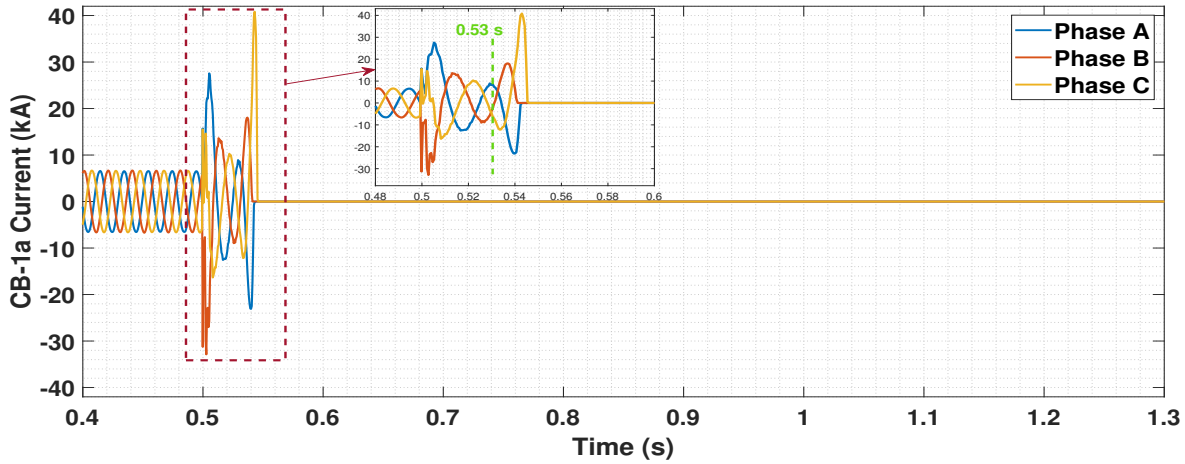

Figure 31. Currents in circuit breaker (CB-1a) upon three-phase line to ground fault in the middle of cable-1.

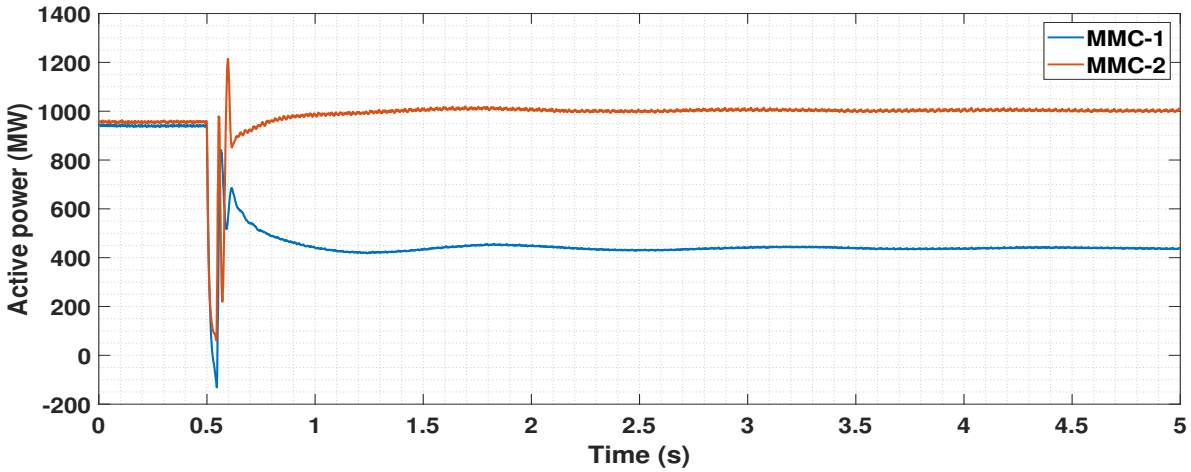

Figure 32. Active power in MMC-1 bus and MMC-2 bus upon three-phase line to ground fault in the middle of cable-1.

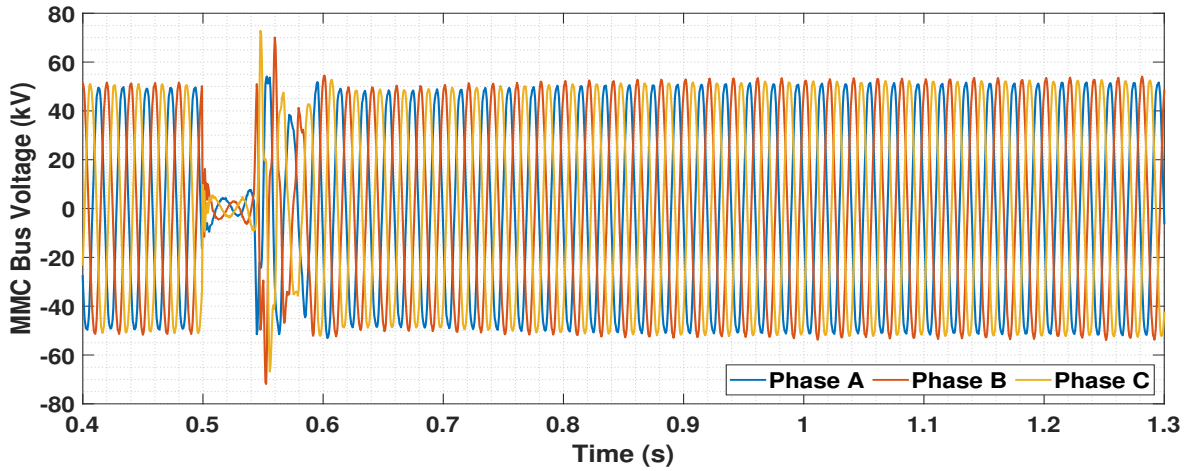

Figure 33. Voltages at MMC bus upon three-phase line to ground fault in the middle of cable-1.

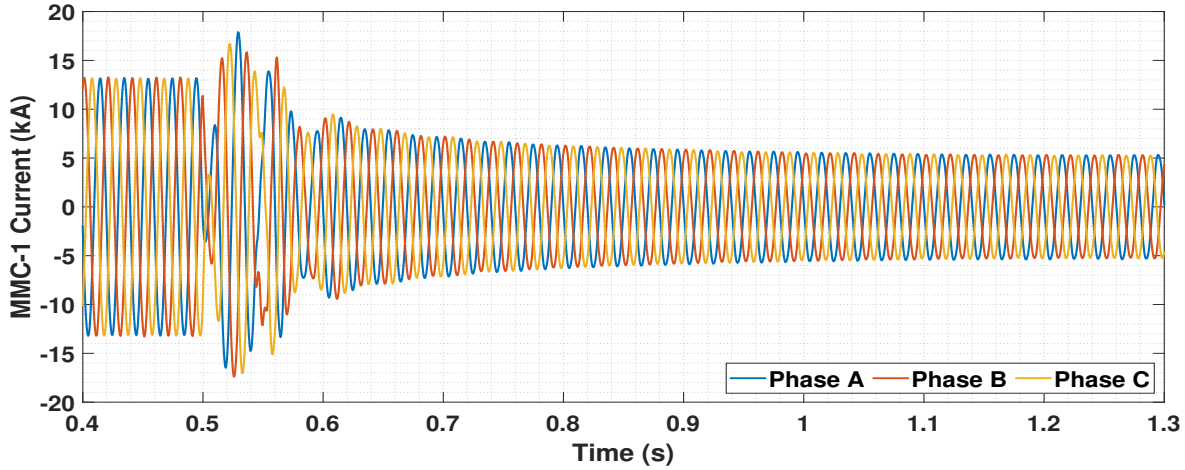

(**a**) Currents in MMC-1 bus

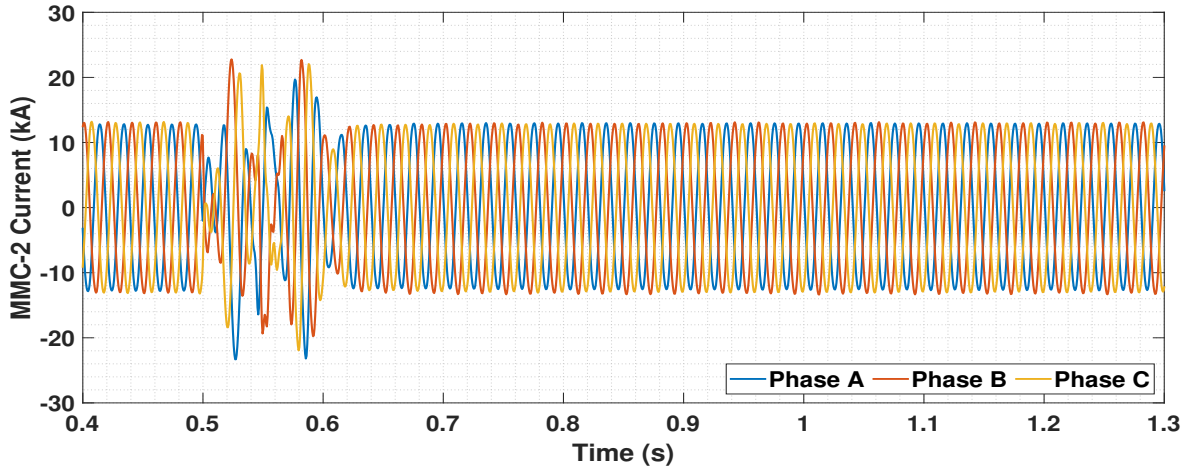

(**b**) Currents in MMC-2 bus

Figure 34. Currents in (**a**) MMC-1 bus and (**b**) MMC-2 bus upon three-phase line to ground fault in the middle of cable-1.

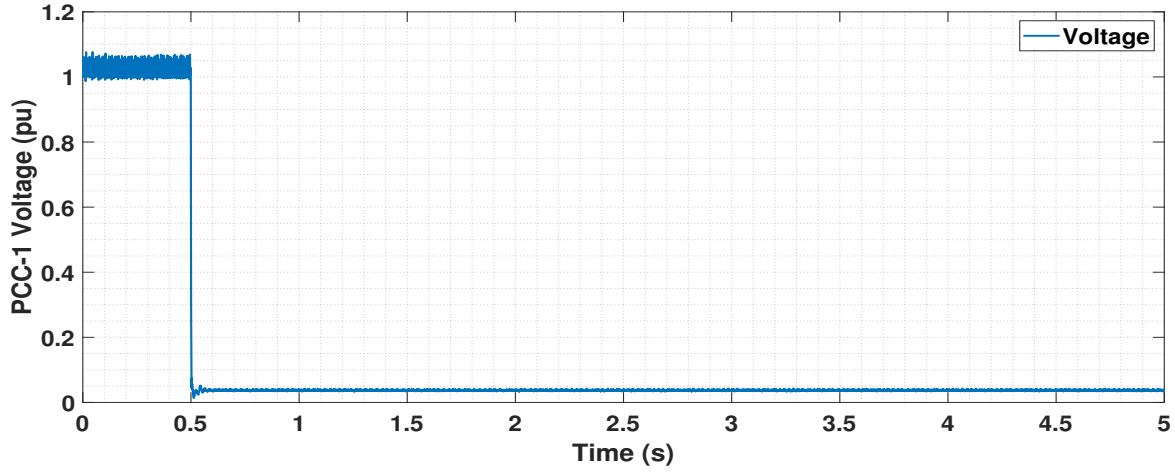

Figure 35. Voltage in p.u. at PCC-1 upon three-phase line to ground fault in the middle of cable-1.

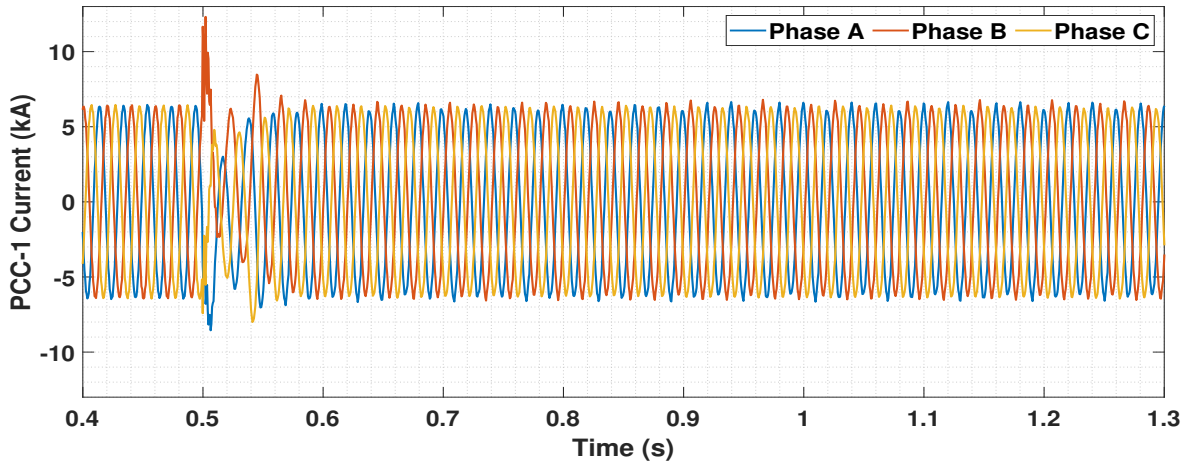

Figure 36. Currents in PCC-1 upon three-phase line to ground fault in the middle of cable-1.

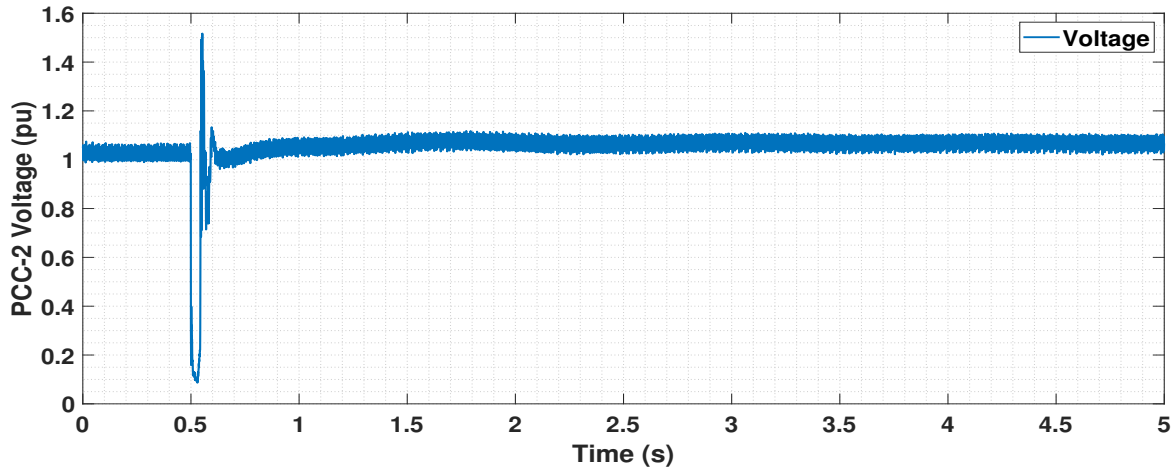

Figure 37. Voltage in p.u. at PCC-2 upon three-phase line to ground fault in the middle of cable-1.

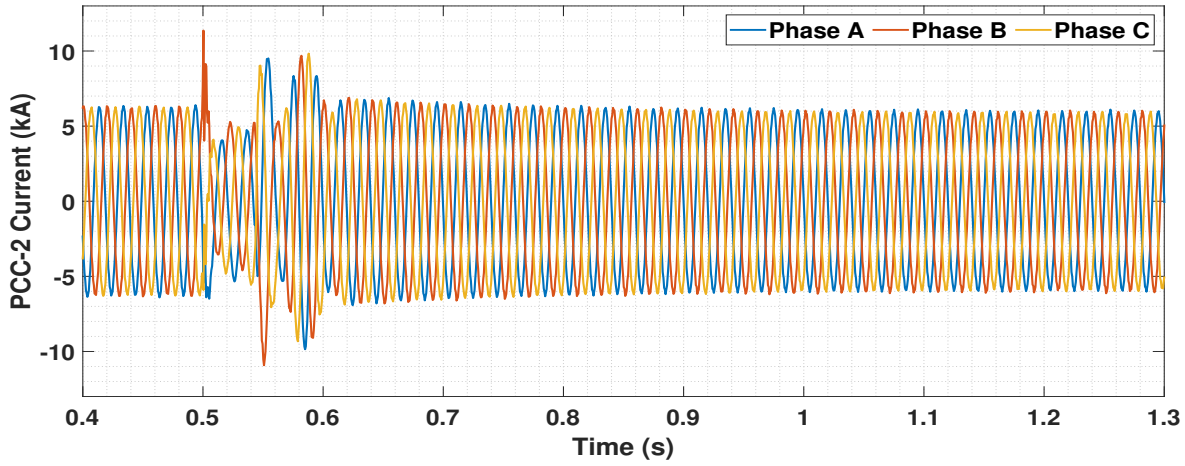

Figure 38. Currents in PCC-2 upon three-phase line to ground fault in the middle of cable-1.

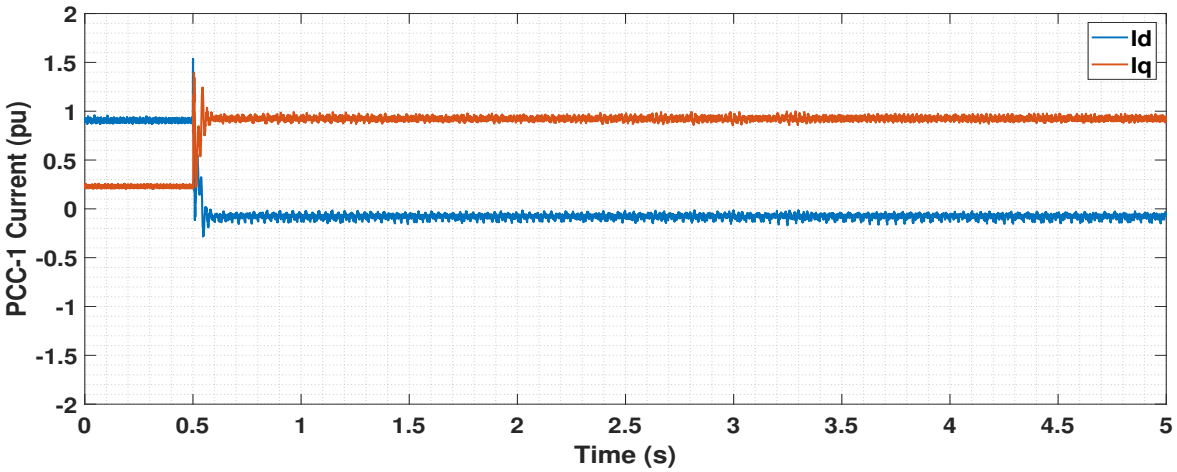

Figure 39. Currents in d and q axes in PCC-1 upon three-phase line to ground fault in the middle of cable-1.

Increase in active power in MMC-2 after the fault has been cleared, can be explained by viewing the current profiles in the OWFs detailed in the following paragraph. A major observation can be derived from the profile of transients during the fault in the currents of both the MMCs in Figure 34a,b. The initial rise in current till 0.53 s is due to the occurrence of the three-phase fault. The breaker is opened at 0.542 s. The profile of currents at nearly 0.59 s are complementary in both MMCs, i.e., the currents are decreasing in MMC-1 and increasing in MMC-2. This is due to the difference in control strategies in MMC-1 (V/F control) and MMC-2 (active power control).

Analyzing at the OWFs side of the network, the DVC is modelled to provide rated reactive current to flow to the fault location by controlling the voltage of the GSC. From the voltage in p.u. in Figure 35, it can be seen that the voltage at the PCC-1 drops and remains low throughout the fault period. During the time of fault in cable-1 and after CB-1a is opened, the voltage angle and magnitude at PCC-1 goes to zero. The PLL in GSC-1 is synchronized with the AC voltage at PCC-1. The voltage magnitude at GSC-1 remains non-zero, and the voltage angle is zero during the time of fault as the PLL follows the angular reference at PCC-1. Therefore, due to higher voltage magnitude at GSC-1 than at PCC-1, reactive power will flow from GSC-1 to PCC-1, and since the voltage angle is zero at GSC-1 and PCC-1, active power transmitted is zero during the time of the fault. This is performed in DVC by controlling the d-axis reference voltage of GSC-1 and thereby indirectly controlling the current coming out of the GSC-1 to PCC-1. The current limitation algorithm implemented in the DVC limits the output current to the rating of the converter and hence rated reactive current flows from the GSC-1 as seen in Figure 36.

Voltages at PCC-2, 3 and 4 have transients during the time of fault and are then stabilized to a slightly higher value than the pre-fault state to compensate for the loss of OWF-1. This is due to the fast local voltage control in DVC as seen for the case of disconnection of one OWF. The post-fault voltage value is within the tolerance limit ($\pm$10%), and it can be viewed from the graphs in Figure 37. An important observation in the voltage graphs of OWFs-2, 3 and 4 is the occurrence of spikes right after the circuit breaker CB-1a is opened, as can be seen in Figure 37. There can be two reasons for such a phenomenon to occur. The first is that after the circuit breaker CB-1a is opened, reactive current injection still takes place (at 0.59 s in Figure 38 for PCC-2) and this causes the voltage at the corresponding PCC also to rise. Such a rise in voltage is not applicable in real-world OWFs and is, therefore, a drawback due to the OWF modelling. These spikes can be ignored as they do not represent the performance of the real hardware. The second reason could be due to two control strategies that provide the voltage reference in the network. It is seen that during the steady state and post-fault condition, the V/F control is dominant and provides the voltage reference in the network. However, during the time of the fault, DVC in all OWFs takes the role of providing the voltage reference in the

corresponding PCCs, as seen in PCC-1 during the time of three-phase line to ground fault in cable-1. The sudden change back to the steady state condition after the fault is released could lead to discrepancies between the V/F mode and the DVC. The conflict between these control strategies occur as to which control strategy provides the voltage reference right after the circuit breaker is open and hence this causes a spike in voltage at the PCCs.

The currents from the OWFs-2, 3 and 4 are the same in the post-fault region as the pre-fault condition (Figure 38 for PCC-2) since the scaling factor for each OWF is still the same. DVC control in these OWFs operate during the time of fault and limit the currents by controlling the voltages at corresponding PCCs. Due to the increase in voltage in the post-fault period at the PCCs-2, 3 and 4, the active power generated also will be higher from the OWFs-2, 3 and 4. It is reflected in the increase in active power in MMC-2 as shown in Figure 32. Another important observation is in the profile of transients in currents in PCCs-2, 3 and 4 following the occurrence of the fault. As shown in Figure 38 for PCC-2, the current is limited from 0.5 to 0.54 s during the time of fault. After the breaker has been operated at 0.542 s, the profile of currents (from 0.55 s to 0.6 s) is similar to that of the MMC-2 (Figure 34b). This is due to the re-synchronization to the grid by the PLL in MMC-2 control and the PLL in DVC of WG-2, 3 and 4.

In practice, if a three-phase fault occurs in a subsea cable, it is hardly that the fault clears on its own and it would require human interference. During such critical islanding situations, the DVC allows rated reactive current to flow to the fault location by controlling the GSC voltage and thereby protecting the converters in the OWF from high overcurrents. Based on the reference grid codes mentioned in [8], during steady state operation, the active current must be the priority, and during the time of the fault, the priority must be changed to reactive current. The major takeaway is that the DVC follows the reactive current injection requirement during the time of the fault, as shown from the currents in PCC-1 in Figure 39, even while working in coordination with other control strategies in the network. Current is limited to the rated current of the converter by the current limitation algorithm in DVC without the requirement of any external controls.

6. Conclusions

In this paper, the development of a large scale EMT model of a 2 GW offshore network in RSCAD is explained in detail. The modifications in the control structures of the MMCs to work in coordination with the implemented DVC in WGs are addressed. The operation of the developed large scale 2 GW network is discussed. The interplay of offshore MMCs and Type-4 WGs in terms of dynamic power flow control within the offshore network (by analyzing the voltage and current profiles in the electrical path between the WGs and the MMCs) is performed. The coordination between the V/F control in MMC-1, active power control in MMC-2 and the DVC in OWFs provide a synchronized operation during the steady state and dynamic conditions in the network. One of the highly severe conditions is the disconnection of one OWF. In that situation, it is observed that the network remains stable following the disconnection and the power flowing through MMC-1 reduces as it is working in V/F control, i.e., capable of providing and absorbing power. Another highly severe event is the three-phase line to ground fault in one of the HVAC cables. A circuit breaker logic is modelled to isolate OWF-1 from the network when the fault occurs in HVAC cable-1. It is observed that the operation of the entire network remains stable during the pre-fault condition where active current is injected, or can be termed as active power generated by all the OWFs. During the time of fault in HVAC cable-1, circuit breaker at the end of the cable is opened upon detection of overcurrent and thereby, islanding OWF-1. The fast local voltage control in DVC in OWF-1 provides voltage support during the time of the fault, and due to the grid conditions, the reactive current is injected by OWF-1 to the fault location. The currents are limited to the current rating of the GSC to avoid the damage of the components in the converter. Hence, it can be concluded that the V/F control provides the voltage reference during the pre-fault and post fault condition for the network and DVC provides voltage reference at the corresponding PCC when the OWF

is islanded. Such a generic model provides scope for expansion to a larger scale of 4 GW. The practicality of the DVC can be tested by performing Hardware In Loop testing of the implemented DVC in a properly set-up test bench. The model also allows to incorporate other control strategies, and studies related to the interoperability of these controllers, coordination with MMC control strategies and higher order contingencies (for e.g., short circuit of two or more WGs, disconnection of two or more WGs) can be performed as future work.

Author Contributions: Conceptualization, S.G., A.P. and J.R.T.; formal analysis, S.G., A.P. and J.R.T.; investigation, S.G., A.P. and J.R.T.; methodology, S.G., A.P. and J.R.T.; resources, S.G., A.P. and J.R.T.; software, S.G., A.P. and J.R.T.; supervision, J.R.T., A.P., A.L., P.P. and M.v.d.M.; validation, S.G., A.P. and J.R.T.; visualization, S.G., A.P. and J.R.T.; writing—original draft, S.G., A.P. and J.R.T.; writing—review & editing, S.G., A.P., A.L., J.R.T., P.P and M.v.d.M. All authors have read and agreed to the published version of the manuscript.

Funding: This research received no external funding.

Data Availability Statement: Data sharing not applicable.

Acknowledgments: This research was fully funded by Delft University of Technology. The authors thank the experts and technical support staff of RTDS Technologies Inc. and DIgSILENT GmbH for the insightful discussions during the execution of this research.

Conflicts of Interest: The authors declare no conflict of interest. The funders had no role in the design of the study; in the collection, analyses, or interpretation of data; in the writing of the manuscript, or in the decision to publish the results.

References

1. UNFCCC. Adoption of the Paris agreement. COP. In *25th Session Paris*; UNFCCC: Rio de Janeiro, Brazil; New York, NY, USA, 2015; Volume 30. Available online: https://unfccc.int/sites/default/files/english_paris_agreement.pdf (accessed on 29 January 2021).
2. Vision—North Sea Wind Power Hub. 2020. Available online: https://northseawindpowerhub.eu/vision/ (accessed on 26 January 2021).
3. TenneT Develops First 2 GW Offshore Grid Connection with Suppliers. *Daily Offshore Wind News*, 13 February 2020.
4. The First Hub-and-Spoke Energy Island—North Sea Wind Power Hub. 2020. Available online: https://northseawindpowerhub.eu/the-first-hub-and-spoke-energy-island/ (accessed on 26 January 2021).
5. Bolik, S.; Ebner, G.; Elahi, H.; Gomis Bellmunt, O.; Hjerrild, J.; Horne, J.; Kilter, J.; Rimez, J.; Temtem, S.; Visiers Guixot, M. HVDC Connection of Offshore Wind Power Plants; Technical Brochure 619; CIGRE Working Group B4.55. 2015. Available online: https://e-cigre.org/publication/619-hvdc-connection-of-offshore-wind-power-plants (accessed on 29 January 2021).
6. Peralta, J.; Saad, H.; Dennetière, S.; Mahseredjian, J.; Nguefeu, S. Detailed and Averaged Models for a 401-level MMC-HVDC system. *IEEE Trans. Power Deliv.* **2012**, *27*, 1501–1508. [CrossRef]
7. Telaretti, E.; Graditi, G.; Ippolito, M.; Zizzo, G. Economic feasibility of stationary electrochemical storages for electric bill management applications: The Italian scenario. *Energy Policy* **2016**, *94*, 126–137. [CrossRef]
8. Mohseni, M.; Islam, S.M. Review of international grid codes for wind power integration: Diversity, technology and a case for global standard. *Renew. Sustain. Energy Rev.* **2012**, *16*, 3876–3890. [CrossRef]
9. *HVDC Technology for Offshore Wind is Maturing*; ABB: Zürich, Switzerland, 2018. Available online: https://new.abb.com/news/detail/8270/hvdc-technology-for-offshore-wind-is-maturing (accessed on 26 January 2021).
10. Korai, A.W. Dynamic Performance of Electrical Power Systems with High Penetration of Power Electronic Converters: Analysis and New Control Methods for Mitigation of Instability Threats and Restoration. Ph.D. Thesis, Universität Duisburg-Essen, Duisburg, Germany, 2019. [CrossRef]
11. Lescale, V.; Holmberg, P.; Ottersten, R.; Hafner, Y. Parallelling offshore wind farms HVDC ties on offshore side. *Proc. CIGRE 2012* **2012**.
12. Ganesh, S.; Perilla, A.; Torres, J.; Palensky, P.; van der Meijden, M. Validation of EMT Digital Twin Models for Dynamic Voltage Performance Assessment of 66 kV Offshore Transmission Network. *Appl. Sci.* **2021**, *11*, 244. [CrossRef]
13. RTDS Technologies Inc. Novacor. 2020. Available online: https://knowledge.rtds.com/hc/en-us/articles/360034290474-NovaCor- (accessed on 26 January 2021).
14. Vrana, T.K.; Yang, Y.; Jovcic, D.; Dennetière, S.; Jardini, J.; Saad, H. The CIGRE B4 DC grid test system. *Electra* **2013**, *270*, 10–19.
15. World's Most Powerful Offshore Wind Turbine: Haliade-X 12 MW | GE Renewable Energy. 2020. Available online: https://www.ge.com/renewableenergy/wind-energy/offshore-wind/haliade-x-offshore-turbine (accessed on 26 January 2021).
16. RTDS Technologies Inc. PB5 Card. 2020. Available online: https://knowledge.rtds.com/hc/en-us/articles/360034285894-PB5-Card (accessed on 26 January 2021).

17. Ryndzionek, R.; Sienkiewicz, L. Evolution of the HVDC Link Connecting Offshore Wind Farms to Onshore Power Systems. *Energies* **2020**, *13*, 1914. [CrossRef]
18. CIGRE Working Group B4.37. VSC Transmission. Technical Brochure 269. 2005. Available online: https://e-cigre.org/publication/269-vsc-transmission (accessed on 26 January 2021).
19. RTDS Technologies Inc. MMC Modeling. 2020. Available online: https://knowledge.rtds.com/hc/en-us/articles/360039628773-MMC-Modeling (accessed on 26 January 2021).
20. Sharifabadi, K.; Harnefors, L.; Nee, H.P.; Norrga, S.; Teodorescu, R. *Design, Control, and Application of Modular Multilevel Converters for HVDC Transmission Systems*; John Wiley & Sons: Hoboken, NJ, USA, 2016.
21. Erlich, I.; Korai, A.; Neumann, T.; Koochack Zadeh, M.; Vogt, S.; Buchhagen, C.; Rauscher, C.; Menze, A.; Jung, J. New Control of Wind Turbines Ensuring Stable and Secure Operation Following Islanding of Wind Farms. *IEEE Trans. Energy Convers.* **2017**, *32*, 1263–1271. [CrossRef]
22. CIGRE Working Group B4.57. Guide for the Development of Models for HVDC Converters in a HVDC Grid. Tech. Rep. 2014. Available online: https://e-cigre.org/publication/604-guide-for-the-development-of-models-for-hvdc-converters-in-a-hvdc-grid (accessed on 26 January 2021).
23. Saad, H.A. ModÉlisation et Simulation D'Une Liaison Hvdc de Type Vsc-Mmc. Ph.D. Thesis, Polytechnique Montréal, Montreal, QC, Canada, 2015.
24. RTDS Technologies Inc. RSCAD Modules. 2020. Available online: https://knowledge.rtds.com/hc/en-us/articles/360037537653-RSCAD-Modules (accessed on 26 January 2021).